Impact of the Valence Band Structure of Cuprous Oxide for Excitons in Quantum Wells

Bachelor thesis from

Frieder Pfeiffer

16.03.2023

Examiner: Prof. Dr. Jörg Main

Vorgelegt an der

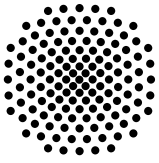

Universität Stuttgart

Institut für Theoretische Physik I
Pfaffenwaldring 57, 70569 Stuttgart

Contents

1 Introduction

Excitons are quasiparticles that can occur in insulators and semiconductors. Their postulation in 1930 by Frenkel [**1**], Peierls [**2**], and Wannier [**3**] was of great theoretical interest regarding the optical properties of these solids. In 1952, excitons in Cu_2O were discovered experimentally by Gross and Karryev [**4**]. The choice of this solid followed, among other things, from the already widely researched electrical properties of Cu_2O. Also, due to a publication in 2014 by the Bayer Group of the Technical University of Dortmund [**5**], excitons are still part of the latest research. The experimental determination of exciton states in Cu_2O up to quantum numbers of $n = 25$, illustrated in fig.1.1, was unique to date and amplified the research interest. Since then, the Institute for Theoretical Physics I (ITP1) at the University of Stuttgart has also been working continuously on excitons in Cu_2O. A hydrogen-like Hamiltonian served as a first approximation for the theoretical description of the exciton states. This approximation already explains the rough form of the Rydberg series shown in fig.1.1. Since a description of the exciton states without considering the crystal is trivially not exact, this Hamiltonian was modified via the band structure of the crystal. Since the analytical solution of the simplified model system is well known, the research of ITP1 was mainly concerned with excitons in the bulk. The bulk refers to a three-dimensional, and arbitrarily far-reaching crystal structure. Since excitons in the bulk are now already extensively researched, see for example in the Ph.D. thesis of Frank Schweiner [**6**], an additional potential was introduced for new insights.

The so-called Quantum Wells correspond to an infinite potential well, which spatially limits one dimension of the crystal. Again a hydrogen-like description, containing the quantum wells was considered first. A programme implemented by Pavel Belov [**7**] serves to solve the exciton states with included Quantum Wells. A previous bachelor thesis by Leon Kühner [**8**] already dealt with the solution of the hydrogen-like model with Quantum Wells. In his bachelor thesis, Niklas Scheuler is currently optimising the programme to reduce the required CPU time and memory. This bachelor thesis is focused on an analytical reduction of the degrees of freedom of the Hamiltonian containing Quantum Wells and the band structure corrections. Combined with the parallel work of Niklas Scheuler, this should make it possible to extend the programme to solving the exciton states with the band structure and the Quantum Wells. The reduction of the degrees

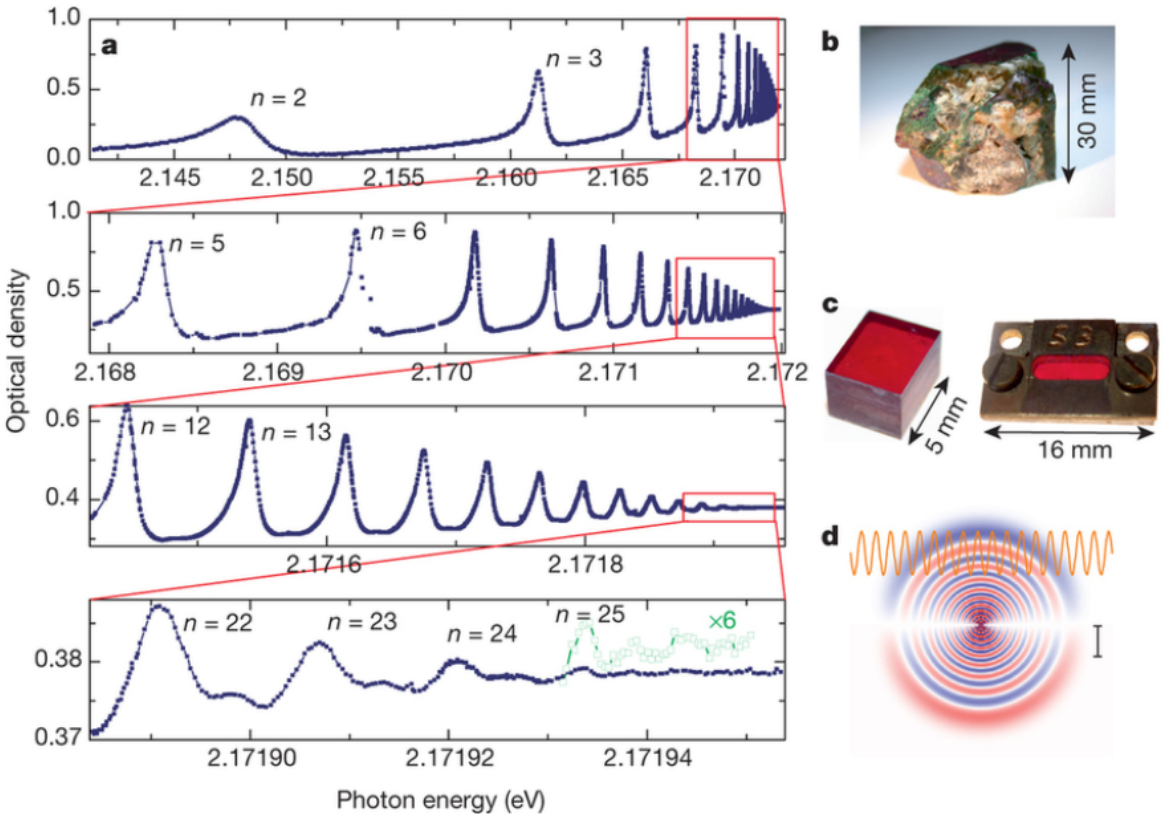

Figure 1.1: (a) Absorption spectrum of the yellow exciton series in Cu_2O. Optical density plotted against the energy of the photons required for excitation. The maxima correspond to resonant energies of different quantum numbers n. (b) Naturally occurring Cu_2O ore. (c) Pure Cu_2O crystal and experimental sample. (d) Wave function of an exciton with quantum number $n = 25$ [**5**].

of freedom was realised by transforming the Hamiltonian into cylindrical coordinates using the existing translation and rotation symmetries. The calculation was checked by Mathematica as well as by a symmetry test of the resulting Hamiltonian. Finally, a basis for the numerical diagonalisation of the Hamiltonian was sketched to give an outlook on future research. Future results by the Giessen group, from the 4th Physical Institute at the University of Stuttgart, will serve as a falsification test for the theoretical discoveries.

2 Solid State Basics

The following sections 2.1 to 2.5 are based on References **[6, 8-10]**.

2.1 Crystals

Based on their external appearance, solids can be divided into two classes. On the one hand, there are crystals, which have a regular, ordered atomic structure and thus also a regular outer appearance. On the other hand, amorphous solids have a disordered atomic structure and thus a disordered appearance. The following considerations are limited to crystalline solids. The underlying atomic structure is referred to in the following as the base. A base can consist of one or more atoms. Single-atomic bases are called primitive, multi-atomic bases are called non-primitive. Furthermore, a base must be constructed in such a way that an arrangement of several identical bases can cover the space inside the crystal completely and without overlap. The shape of a base is therefore dependent on the atomic structure of a crystal and is closely related to its symmetry properties. The periodic, regular arrangement of the bases in a crystal motivates the introduction of a periodic lattice. The bases are mapped onto points, and thus the crystal is represented by a periodic point lattice. This separation simplifies further analysis of the crystal.

2.2 Crystal Symmetry

Crystal symmetries are of particular interest. We are therefore looking for operations that hold the point lattice invariant. Possible operations are translations, rotations, reflections, and inversions. First consider the translation symmetry, where an arbitrary point $\boldsymbol{r}$ is chosen within the crystal. Let the environment of $\boldsymbol{r}$ be $U(\boldsymbol{r})$. If one shifts the point $\boldsymbol{r}$ by the lattice vector

$$\boldsymbol{R} = n_1\boldsymbol{a_1} + n_2\boldsymbol{a_2} + n_3\boldsymbol{a_3}, \tag{2.1}$$

Table 2.1: A primitive Bravais lattice exists for each of the seven crystal systems. They are distinguished by the lengths a, b, c and the angles α, β, γ of the basis vectors relative to each other. The order of rotation corresponds to the number of rotational axes.

crystal system	lattice constants	angles	rotational axes
triclinic	$a \neq b \neq c$	$\alpha \neq \beta \neq \gamma$	1
monoclinic	$a \neq b \neq c$	$\alpha = \gamma = 90°, \beta \neq 90°$	2
orthorombic	$a \neq b \neq c$	$\alpha = \beta = \gamma = 90°$	2
tetragonal	$a = b \neq c$	$\alpha = \beta = \gamma = 90°$	4
hexagonal	$a = b \neq c$	$\alpha = \beta = 90°, \gamma = 120°$	6
trigonal	$a = b = c$	$\alpha = \beta = \gamma < 120° \neq 90°$	3
cubic	$a = b = c$	$\alpha = \beta = \gamma = 90°$	3

one again ends up in an identical environment

$$U(\boldsymbol{r}) = U(\boldsymbol{r} + \boldsymbol{R}). \tag{2.2}$$

The basis vectors $\boldsymbol{a_1}, \boldsymbol{a_2}$, and $\boldsymbol{a_3}$ form a coordinate system that spans the crystal lattice. The lengths $|\boldsymbol{a_1}| = a, |\boldsymbol{a_2}| = b, |\boldsymbol{a_3}| = c$ and angles α, β, γ of the basis vectors relative to each other can be used to construct different lattices. Taking into account the properties of a base (2.1), 14 Bravais lattices are possible in three-dimensional space. For seven of the 14 Bravais lattices primitive bases can be found, which represent the seven crystal systems, listed in tab.2.1. The integers n_1, n_2, n_3 serve as a count of the discrete lattice points. Rotation, reflection and inversion belong to the point symmetry. Characteristic of the point symmetry is the fixing of at least one lattice point. A trivial rotation by 2π leads to an identical structure for any grid and is therefore of little interest. More interesting are discrete rotations around $2\pi/n$ with $n \in \{2, 3, 4, 6\}$. The choice for n arises from the requirement of an area-covering and non-overlapping basis. Illustratively, the two-dimensional space can thus be completely covered by triangles, quadrangles and hexagons, but not by pentagons, heptagons or octagons without overlap, as it can be seen in fig.2.1. The same applies to the corresponding polyhedra in three dimensions. Reflection symmetry arises through reflection on a fixed plane and therefore always occurs in the company of rotation symmetry. The inversion projects the position vector $\boldsymbol{r}$ back to its negative $-\boldsymbol{r}$ and thus occurs with every ideal point lattice but not necessarily in the crystal itself. With the three point symmetries, the seven crystal systems can be subdivided into a further 32 crystal classes or point groups. Since the cubic structure of the Cu_2O-crystal has the same point symmetry as the octahedron, it belongs to the O_h point group, see fig.2.2.

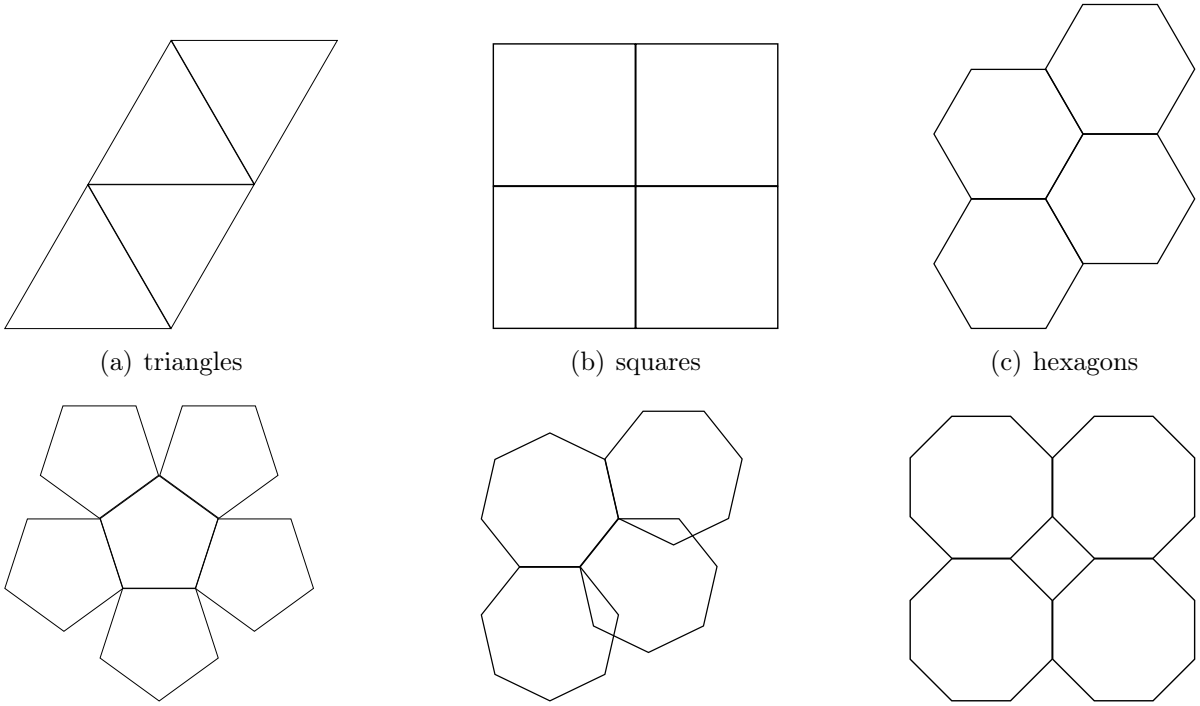

(a) triangles (b) squares (c) hexagons

(d) pentagons (e) heptagons (f) octagons

Figure 2.1: In the first row from left to right, various arrangements of triangles (a), squares (b), and hexagons (c) can be seen. These three geometric forms fulfill the conditons to be a base and therefore the corresponding rotational symmetries can exist. In the second row from left to right, various arrangements of pentagons (d), heptagons (e), and octagons (f) can be seen in two-dimensional space. This results in either unavoidable gaps or overlaps of the individual polygons that are not permitted for bases. Accordingly, corresponding rotational symmetries of order $n = 5, 7, 8$ cannot exist in the crystal lattice.

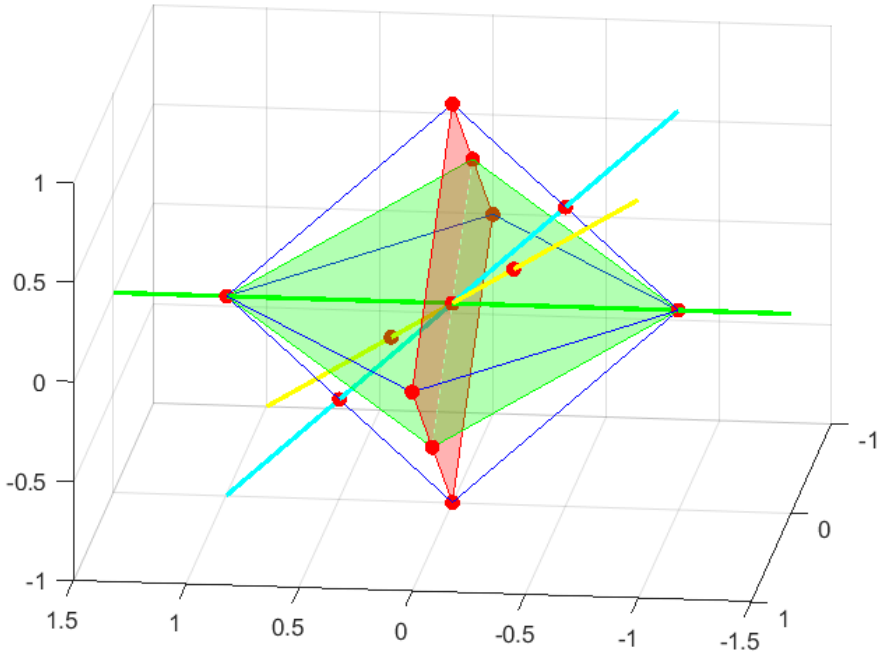

Figure 2.2: The blue edges, red vertices, and intervening faces form a regular polygon, the octahedron. The green straight line through two of the vertices corresponds to one of the three fourfold axes of rotation. The yellow straight line through two centres of opposite faces corresponds to one of the four triple axes of rotation. The cyan straight line through two centres of opposite edges corresponds to one of the six two-count axes of rotation. The nine symmetry planes are composed of three planes each containing four corner points (red) and six planes each containing two corner points and two center points along the edges (green).

2.3 Cuprous Oxide

This section is based on References [**6**, **8**, **11**].

Cu_2O occurs in nature initially as a green-yellowish ore while the pure substance has a reddish appearance as it is shown in fig.1.1. The cubic crystal structure, illustrated in fig.2.3 consists of the mutually displaced superposition of a bcc lattice of oxygen and an fcc lattice of copper. Due to its structure, Cu_2O is in the cubic crystal system and therefore belongs to the O_h group. Thus, Cu_2O has the full octahedral symmetry, i.e. four sixfold rotational mirror axes $4S_6$, three fourfold rotational mirror axes $3S_4$, three fourfold rotational axes $3C_4$, four threefold rotational axes $4C_3$, 6 twofold rotational axes $6C_2$, 9 symmetry planes $3\sigma_n$ and $6\sigma_d$, as well as the inversion I.

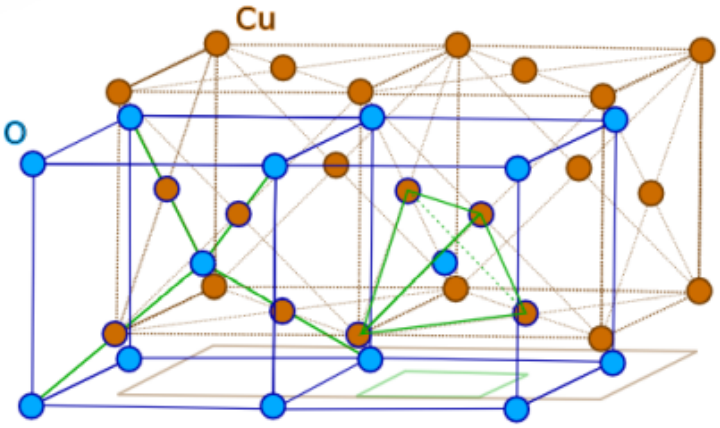

Figure 2.3: Structure of the Cu_2O crystal, consisting of two cubic lattices spatially displaced against each other. The blue lattice occupied by oxygen atoms is body-centered cubic (bcc). The orange lattice occupied by copper atoms is face-centered cubic (fcc) [**12**].

2.4 Reciprocal Lattice

If particles are investigated in periodic potentials $V(\boldsymbol{r}) = V(\boldsymbol{r} + \boldsymbol{R})$, the introduction of reciprocal space is suitable. The reciprocal space or momentum space is spanned by wave vectors $\boldsymbol{k}$. Let a point lattice with the corresponding lattice vector $\boldsymbol{R}$ be given. Furthermore, let the plane wave

$$\psi_{\boldsymbol{k}}(\boldsymbol{r}) = \psi_0 \exp\{i\boldsymbol{k}\boldsymbol{r}\} \tag{2.3}$$

with amplitude ψ_0 be a solution of the stationary Schrödinger equation

$$H\psi = E\psi \tag{2.4}$$

in real space. Then the reciprocal space is spanned by the wave vectors, which correspond to the periodicity of the point lattice. Let the lattice periodic condition

$$\psi_0 \exp\{i\boldsymbol{k}\boldsymbol{r}\} = \psi_{\boldsymbol{k}}(\boldsymbol{r}) = \psi_{\boldsymbol{k}}(\boldsymbol{r} + \boldsymbol{R}) = \psi_0 \exp\{i\boldsymbol{k}(\boldsymbol{r} + \boldsymbol{R})\} \tag{2.5}$$

be fulfilled. To solve this equation the reciprocal lattice vector

$$\boldsymbol{G} = h_1\boldsymbol{b_1} + h_2\boldsymbol{b_2} + h_3\boldsymbol{b_3} \tag{2.6}$$

is introduced. The new basis vectors

$$\boldsymbol{b_1} = \frac{2\pi}{\boldsymbol{a_1} \cdot (\boldsymbol{a_2} \times \boldsymbol{a_3})} \boldsymbol{a_2} \times \boldsymbol{a_3},$$

$$\boldsymbol{b_2} = \frac{2\pi}{\boldsymbol{a_1} \cdot (\boldsymbol{a_2} \times \boldsymbol{a_3})} \boldsymbol{a_3} \times \boldsymbol{a_1}, \tag{2.7}$$

$$\boldsymbol{b_3} = \frac{2\pi}{\boldsymbol{a_1} \cdot (\boldsymbol{a_2} \times \boldsymbol{a_3})} \boldsymbol{a_1} \times \boldsymbol{a_2},$$

in the reciprocal space follow directly from the condition

$$\exp\{i\boldsymbol{kR}\} = \exp\{i\boldsymbol{GR}\} = 1, \tag{2.8}$$

and equation (2.6), while h_1, h_2, h_3 take integer values. The value of the scalar triple product $\boldsymbol{a_1} \cdot (\boldsymbol{a_2} \times \boldsymbol{a_3}) = V$ corresponds to the volume V of the unit cell in the real space. It is now suitable to introduce a geometric construction into the newly created point lattice. The Wigner Seitz cell, see fig.2.4 is now a monatomic basis, which after construction covers all points that have the smallest distance to its own base atom. The Wigner Seitz cell in reciprocal space is also called the first Brillouin zone.

2.5 Quasi Free Electrons and Ideal Band Structure

First consider a free electron gas in the volume $V = L_1 L_2 L_3$ of the solid. The electrons are assumed to be mobile and the particle interaction is neglected. Assuming that N electrons are enclosed in the volume V at a negligible temperature T, the many-particle Hamiltonian

$$H = \sum_{l=1}^{N} \frac{\boldsymbol{p}_l^2}{2m_0} \tag{2.9}$$

with electron mass m_0 and momentum operator $\boldsymbol{p}_l$ of a single electron is given. The approach

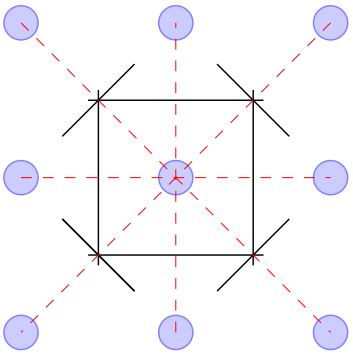

(a) Construction of the Wigner Seitz cell in two dimensions

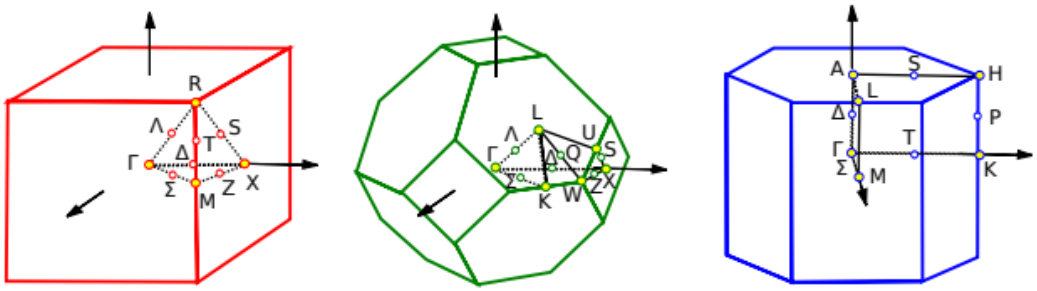

(b) Various Wigner Seitz cells in three dimensions with points of high symmetry

Figure 2.4: (a) The construction of the Wigner Seitz cell for a cubic crystal lattice in two-dimensional space is shown. The dashed, red lines connect the center of the cell with the nearest neighboring atoms. The black lines bisect the connecting lines and thus enclose all points nearest to the center. By definition, the enclosed area is the Wigner Seitz cell. (b) From left to right the three-dimensional Wigner Seitz cells of a simple cubic cell, a diamond-type cell, and a hexagonal cell are shown. The marked points correspond to points of high symmetry **[6]**.

$$\Psi(\{\boldsymbol{r}_l\}_{l=1,\dots,N}) = \prod_{l=1}^{N} \psi(\boldsymbol{r}_l) \tag{2.10}$$

with total wave function $\Psi(\{\boldsymbol{r}_l\}_{l=1,\dots,N})$ and the wave functions $\psi(\boldsymbol{r}_l)$ of single electrons reduces the problem to the stationary single-particle Schrödinger equation

$$H_l\psi(\boldsymbol{r}_l) = \frac{\boldsymbol{p}_l^2}{2m_0}\psi(\boldsymbol{r}_l) = E_l\psi(\boldsymbol{r}_l) \tag{2.11}$$

with energy eigenvalues E_l of the electron. Let the solution be a plane wave

$$\psi_{\boldsymbol{k}}(\boldsymbol{r}) = \frac{1}{\sqrt{V}} \exp\{i\boldsymbol{k}\boldsymbol{r}\} \tag{2.12}$$

with the normalisation

$$\int_V |\psi_{\boldsymbol{k}}(\boldsymbol{r})|^2 d\boldsymbol{r} = 1. \tag{2.13}$$

The parabolic energy eigenvalues

$$E_l(\boldsymbol{k}) = \frac{\hbar^2\boldsymbol{k}^2}{2m_0} \tag{2.14}$$

with Planck's constant $\hbar$ result. The allowed energy states are thus classified by the wave vector $\boldsymbol{k}$. The periodic boundary conditions

$$\psi(\boldsymbol{r}_l) = \psi(\boldsymbol{r}_l + \boldsymbol{L}) \tag{2.15}$$

caused by the edge of the volume V lead to discrete values $k_i = 2\pi n_i/L_i$ with $i \in \{1,2,3\}$. Thus, n_i is an integer and, analogously to $\boldsymbol{k}$, describes the allowed states and energy eigenvalues

$$E_n = \frac{\hbar^2}{2m_0}\sum_{i=1}^{3}\frac{(2\pi)^2}{L_i^2}n_i^2 \tag{2.16}$$

of the electrons. Since electrons are fermions and therefore obey the Pauli principle, each of these states can be occupied by two electrons of different spin. In the ground

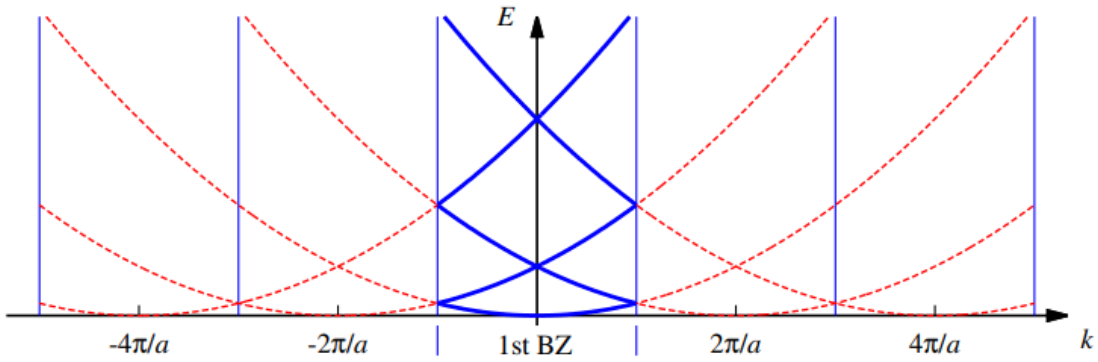

Figure 2.5: Representation of the energy bands of quasi-free electrons. The band structure in one-dimensional lattice with negligible potential is shown. The energy eigenvalues $E(k)$ have a periodicity of $2\pi/a$. The reduction of the band structure to the first Brillouin zone $-\pi/a < k < \pi/a$ is highlighted in blue **[6]**.

state with temperature $T = 0$, the energy levels are filled according to increasing energy. The maximum occupied state corresponds to the Fermi energy E_f. The possible electron states $E(\boldsymbol{k})$ form the parabolic band structure of the free electron gas.

As an intermediate consideration, let the electrons be in a vanishing periodic potential $V \approx 0$. From the solution of the free electron gas and the demand for a periodicity of the wave function, periodically repeating energy eigenvalues $E(\boldsymbol{k}) = E(\boldsymbol{k} + \boldsymbol{G})$ follow. If a is the distance between the lattice points in real space, the length of the reciprocal lattice vector is a multiple of $2\pi/a$. As a result, periodic, overlapping energy bands arise, which can be seen fig.2.5. Due to the finite lattice spacing a, the k-vectors within the first Brillouin zone $-\pi/a < k < \pi/a$ cannot be distinguished from the k-vectors with $|k| \geq \pi/a$. For the complete description, it is therefore sufficient to consider the band structure reduced to the first Brillouin zone.

Let the electron gas now be in a finite crystal. For the theoretical description, it is suitable to introduce a periodic potential

$$V(\boldsymbol{r}_l) = V(\boldsymbol{r}_l + \boldsymbol{R}) \tag{2.17}$$

caused by the crystal structure. Furthermore, the Coulomb interaction of the electron with the remaining charges is also taken into account. The result is the Hamiltonian

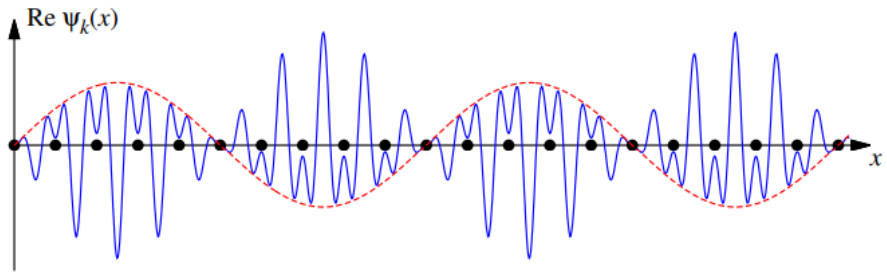

Figure 2.6: Image of the one-dimensional Bloch function. Shown is the real part of the Bloch function $\mathrm{Re}(\psi_\mathrm{k})$. The containing lattice periodic function $u_\mathrm{k}(x)$ is responsible for the finer form of the curve, while the real part of the complex exponential function $\mathrm{Re}(\exp\{ikx\})$ models the red, dashed sine wave. The black dots correspond to the positions of the atoms in the real space [6].

$$H = \sum_{l=1}^{N}\left(\frac{\boldsymbol{p}_l}{2m_0} + V(\boldsymbol{r}_l)\right) + \frac{1}{2}\sum_{\substack{k,l=1\\k\neq l}}^{N}\frac{e^2}{4\pi\epsilon_0|\boldsymbol{r}_l - \boldsymbol{r}_k|} \tag{2.18}$$

with dielectric constant ϵ_0 and elementary charge e. To solve the resulting Schrödinger equation, it is suitable to introduce an effective potential V_eff, which contains both the lattice periodic potential $V(\boldsymbol{r}_l)$ and the Coulomb interaction. Again, the stationary Schrödinger equation (2.4) has to be solved with the Hamilton operator

$$H = \sum_{l=1}^{N}\left(\frac{\boldsymbol{p}_l^2}{2m_0} + V_\mathrm{eff}(\boldsymbol{r}_l)\right). \tag{2.19}$$

It should be mentioned that now the wave function does not describe an electron anymore but a suitable quasiparticle. The Bloch function

$$\psi_{\boldsymbol{k}}(\boldsymbol{r}) = u_{\boldsymbol{k}}\exp\{i\boldsymbol{k}\boldsymbol{r}\} \tag{2.20}$$

is assumed where

$$u_{\boldsymbol{k}}(\boldsymbol{r}) = u_{\boldsymbol{k}}(\boldsymbol{r} + \boldsymbol{R}) \tag{2.21}$$

represents the periodicity of the lattice as shown in fig.2.6. It should be noted that due to Bloch's theorem the product of a complex exponential $\exp\{i\boldsymbol{k}\boldsymbol{r}\}$ and a lattice periodic

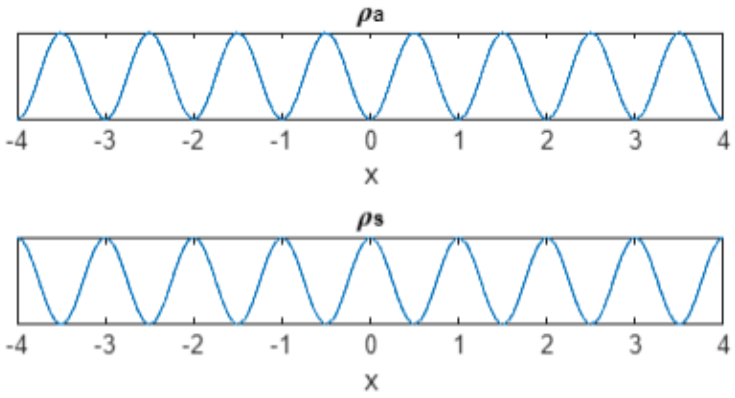

Figure 2.7: Image of the charge density of an electron with the wave vector $k = \pi/a$ in one-dimensional real space. The charge density ρ_s of the electron in the case of a symmetric wave function ψ_s, and the charge density ρ_a of the electron in the case of an antisymmetric wave function ψ_a are shown. The x axis is in units of the lattice constant a, so each integer corresponds to an atom in the lattice.

function $u_{\boldsymbol{k}}(\boldsymbol{r})$ could generally be used to solve periodic potentials. From a shift of the stationary Schrödinger equation

$$H\psi_{\boldsymbol{k}+\boldsymbol{G}}(\boldsymbol{r}) = E_n\psi_{\boldsymbol{k}+\boldsymbol{G}}(\boldsymbol{r}) \tag{2.22}$$

around $\boldsymbol{G}$, the periodicity of the energy eigenvalues $E(\boldsymbol{k}) = E(\boldsymbol{k}+\boldsymbol{G})$ follows as we already assumed for the vanishing potential. Again, periodically repeating energy bands arise. The periodic lattice leads to another effect. The reflection of the wave functions at the lattice points leads to a superposition between the incoming and reflected wave and thus to a standing wave

$$\begin{aligned} \psi_\mathrm{s} &\propto \cos\frac{\pi x}{a}, \\ \psi_\mathrm{a} &\propto \sin\frac{\pi x}{a}. \end{aligned} \tag{2.23}$$

This means that the probability density

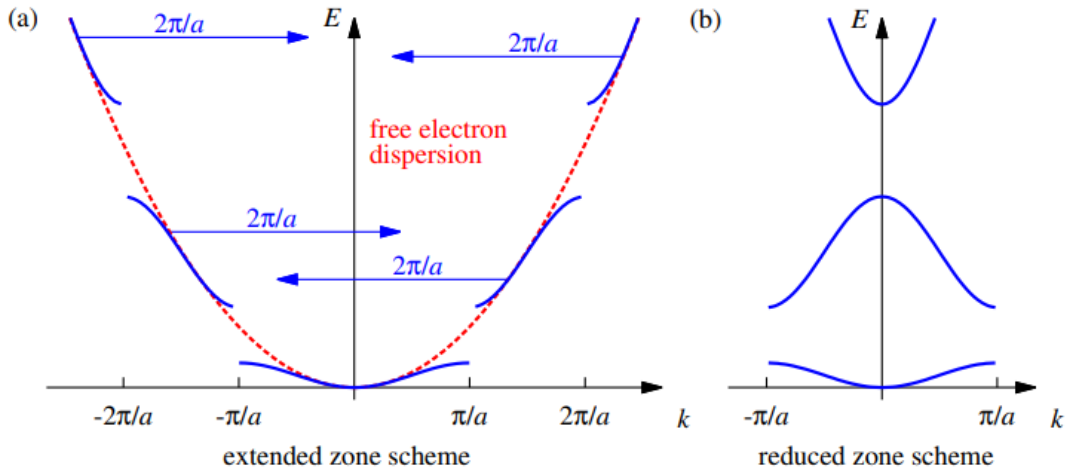

Figure 2.8: (a) Band structure of the one-dimensional lattice with influence of electron scattering and the resulting standing waves. The deviation of the dispersion of free electrons in red from the dispersion of electrons with the influence of the Bragg reflection in blue creates zones of forbidden energies, the band gaps. (b) Reduced zone scheme, created by mapping the bandstructure into the first Brillouin zone [**6**].

$$\rho_\mathrm{s} \propto \cos^2 \frac{\pi x}{a}, \qquad \rho_\mathrm{a} \propto \sin^2 \frac{\pi x}{a}. \tag{2.24}$$

at the lattice points becomes extreme. In the symmetrical case ψ_s, the charge density ρ_s at the lattice points is at its maximum, and thus the energy of the electrons is lowered. In the antisymmetrical case ψ_a, on the other hand, the charge density ρ_a at the lattice points is minimal, and thus the energy of the electrons is increased, see fig.2.7. As a result, the predominant degeneracy of the states is lifted. The resulting gaps illustrated in fig.2.8 in the previously allowed energy spectrum are called band gaps. Now solids can be categorised by the occupation scheme in the ground state and the position of the band gaps relative to the Fermi energy. If the Fermi energy is within a band, one speaks of a conductor, otherwise of a semiconductor or insulator. Semiconductors and insulators differ in the relative distance between the two bands next to the Fermi energy. Larger band gaps are characteristic to insulators, while smaller band gaps belong to semiconductors.

3 Excitons in Cuprous Oxide

Let the semiconductor Cu_2O be given. The bands that are completely occupied in the ground state are called valence bands. The empty bands, on the other hand, are called conduction bands. The band gap E_g, which can be seen in fig.3.1, between the uppermost valence band and the lowermost conduction band prevents a spontaneous exchange of particles between the two bands. However, external excitations, such as light of frequency $\omega = \Delta E/\hbar$, can detach an electron from a valence band and lift it into a conduction band. ΔE corresponds to the energy difference between the two bands. This charge transfer creates a negative charge in the conduction band as well as a positive hole in the valence band. The resulting electron-hole pair can obtain bound states, and is called exciton. It should be noted that the exciton is called a quasiparticle because the hole does not exist as a particle but only has the corresponding properties. Because of their similarity to the hydrogen atom, excitons are assigned to the Rydberg atoms.

3.1 Previous Research

Various analytical and numerical approaches already used to describe exciton states in Cu_2O are presented. A distinction is made between excitons in the bulk and excitons in quantum wells, as well as between a hydrogen-like description and a consideration of the band structure.

In a first approximation, excitons can be described as hydrogen-like. Taking into account the changed parameters, such as the effective masses of electron and hole, bound states analogous to the hydrogen atom result. The time-independent and rotationally symmetric Coulomb potential leads to conservation of energy and angular momentum. The conservation quantities correspond to the later introduced good quantum numbers $\{n, l, m\}$ of the hydrogen atom. Finally, the existing rotational symmetry motivates the introduction of spherical coordinates $\{\rho, \theta, \phi\}$. Altogether, this shows the analogy to the bound states $\psi_{nlm}(\rho, \theta, \phi)$ of the hydrogen atom. These states satisfy the stationary Schrödinger equation (2.4) with the Hamiltonian

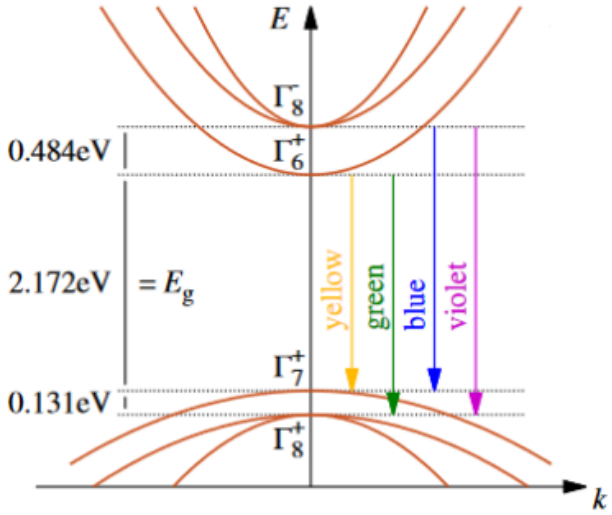

Figure 3.1: Band structure of Cu_2O with band gap $E_g = 2.172$ eV. Shown are the lowest three conduction bands, where Γ_6^+ is single degenerate and Γ_8^- is double degenerate, and the top three valence bands, where Γ_7^+ is single degenerate and Γ_8^+ is double degenerate. The yellow, green, blue, and purple arrows indicate electron transitions, in which light of the corresponding colour is emitted. Note that in the following calculations, yellow excitons corresponding to the yellow light are considered [**11**].

$$H = T_{\mathrm{e}}(\mathbf{p}_{\mathrm{e}}) + T_{\mathrm{h}}(\mathbf{p}_{\mathrm{h}}) + V_{\mathrm{c}}, \tag{3.1}$$

depending on the Coulomb potential V_{c}, the kinetic energy T_{e} of the electron, and the kinetic energy T_{h} of the hole.

Since a description of the excitons without taking the band structure into account is obviously incomplete, this consideration has already been extended by taking the band structure into account. In the bulk, the band structure breaks the previously existing rotational symmetry and thus also the conservation of the orbital angular momentum. As a result, l loses the property of a good quantum number and is replaced by the quantum number j, which also contains the spin-orbit coupling. If we further consider the three-dimensional translational symmetry, the initial six degrees of freedom $\{x_{\mathrm{e}}, y_{\mathrm{e}}, z_{\mathrm{e}}, x_{\mathrm{h}}, y_{\mathrm{h}}, z_{\mathrm{h}}\}$ of electron and hole can be reduced to three degrees of freedom $\{x, y, z\}$, which correspond to the relative coordinates. The Hamiltonian

$$H = T_{\mathrm{e}}(\mathbf{p}_{\mathrm{e}}) + T_{\mathrm{h}}(\mathbf{p}_{\mathrm{h}}, \mathbf{S}_{\mathrm{h}}, \mathbf{I}) + V_{\mathrm{c}} \tag{3.2}$$

thus includes additional corrections to the hole dynamics T_{h}, as well as the spin-orbit coupling of hole spin $\mathbf{S}_{\mathrm{h}}$ and quasispin $\mathbf{I}$.

3.2 Hydrogen Atom

This section is based on References [**13-15**].

A hydrogen-like Hamiltonian, serves as a first approximation to describe the excitons. Therefore, the Rydberg energy

$$E_{n=1} = -\frac{me^2}{32\pi\hbar^2\epsilon_0}\frac{1}{1^2} = -13.6\mathrm{eV} \tag{3.3}$$

and corresponding Bohr radius

$$r_0 = \frac{4\pi\epsilon_0\hbar^2}{me^2} \approx 5.29 \times 10^{-11}\mathrm{m} \tag{3.4}$$

resulting from the solution of the Schrödinger equation of the hydrogen atom are listed. A more detailed calculation for solving the corresponding Schrödinger equation can be found in the appendix A.1. In total, the wave function

$$\psi_{nlm}(r,\theta,\phi) = R_{nl}(r)Y_{lm}(\theta,\phi), \tag{3.5}$$

determined by three quantum numbers n, l, m represents the electron state in the hydrogen atom. The principal quantum number $n \in \mathbb{N}$ essentially determines the energy of the electron. In the ground state $n = 1$, equation (A.21) leads to the already introduced Rydberg energy $E_{\mathrm{H}} = 13.6\mathrm{eV}$ and the Bohr radius $r_0 = 0.529 \times 10^{-10}\mathrm{m}$. The secondary quantum number $l < n, (l \in \mathbb{N})$ represents the magnitude of the orbital angular momentum. The magnetic quantum number $|m| \leq l, (m \in \mathbb{Z})$ describes the projection of the orbital angular momentum onto the z-axis and thus its orientation. The spin $s = \pm 1/2$, which has not occurred so far, is interpreted as the intrinsic angular momentum of the electron. It becomes relevant as soon as several electrons are considered, or also in the case of an orbital coupling. Other possible quantum numbers are described in tab.3.1. In order to describe a quantum state ϕ_i completely, it is sufficient to know its eigenvalues. All eigenvalues q_i are determined via the eigenvalue equations $\boldsymbol{Q}_i\phi_i = q_i\phi_i$, where each operator $\boldsymbol{Q}_i$ corresponds to a quantum number. It is therefore common to describe a quantum mechanical state via a set of quantum numbers. Since this set is generally not unique, good quantum numbers are usually chosen. A set of good quantum numbers is characterized by the fact that their operators commutate with each other in pairs and the representation of the state is unique. Due to the commutativity of the operators, it is possible to determine all observables simultaneously and with arbitrary precision. For the hydrogen atom without spin-orbit coupling, the set $\{n, l, m\}$ contains good quantum numbers, since $\{\mathbf{H}, \boldsymbol{L}^2, \boldsymbol{L}_z\}$ commutate in pairs and the state is uniquely determined via the eigenvalues $\{E_n, l(l+1)\hbar^2, m\hbar\}$. While the electron is in a rotationally symmetric potential, the environment of the exciton is more complex. Both the crystal lattice and the introduced quantum wells destroy the symmetries of the system that are comparable to those of the hydrogen atom. As a consequence, $\{n, l, m\}$ are no longer good quantum numbers and a different set of good quantum numbers is needed to describe the excitons. The coupling $\boldsymbol{J} = \boldsymbol{I} + \mathbf{S}_{\mathrm{h}}$ of hole spin $\mathbf{S}_{\mathrm{h}}$ and quasin spin $\boldsymbol{I}$ caused via the band structure can be considered as a new good quantum number. $\boldsymbol{J}$ is thus the total angular momentum of the hole. Since in general the energy eigenvalues of a system are of special interest, the Hamiltonian is considered first and then a set of good quantum numbers is established in section 4.2.2.

3.3 Bulk Excitons in Cuprous Oxide

Taking the band structure into account, the hydrogen-like Hamiltonian (3.1) must be modified. The main differences between excitons in Cu_2O and the hydrogen atom are,

Table 3.1: Quantum numbers important for the hydrogen atom and the later evaluation, as well as the corresponding operators and eigenvalues. The operators with the index z each stand for the corresponding projections on the z axis.

operator	eigenvalue	quantum number	values
$\boldsymbol{H}$	E_n	n	$n \in \mathbb{N}$
$\boldsymbol{L}^2$	$l(l+1)\hbar^2$	l	$0 \leq l < n$
$\boldsymbol{L}_z$	$m_l\hbar$	m_l	$\lvert m_l\rvert \leq l$
$\boldsymbol{S}^2$	$s(s+1)\hbar^2$	s	$s = 1/2$
$\boldsymbol{S}_z$	$m_s\hbar$	m_s	$\lvert m_s\rvert \leq s$
$\boldsymbol{J}^2$	$j(j+1)\hbar^2$	j	$j \in \{\lvert l-s\rvert, ..., \lvert l+s\rvert\}$
$\boldsymbol{J}_z$	$m_j\hbar$	$m_j = m_s + m_l$	$\lvert m_j\rvert \leq j$

among other things, the effective masses of the charge carriers. Effective hole and electron mass of excitons are determined by the band structure. In the following, the different exciton states are described via the colour corresponding to the excitation. If the hole is in the Γ_7^+ band, one speaks of a yellow exciton, if the hole is in the Γ_8^+ band, one speaks of a green exciton, see fig.3.1. While the effective electron mass results in $m_\mathrm{e} = 0.99m_0$ **[16]**, the effective hole mass is $m_\mathrm{h} = 0.69m_\mathrm{e}$ for the yellow exciton, and $m_\mathrm{h} = 0.58m_\mathrm{e}$ for the green exciton. So while the electron mass is approximately the same as for the hydrogen atom, the hole and proton mass differ significantly. Besides the replaced effective masses, the Hamiltonian (3.2) contains additional correction terms of the hole dynamics, in which, among other things, the spin-orbit coupling between hole spin $\boldsymbol{S}_\mathrm{h}$ and quasispin $\boldsymbol{I}$ is included.

As a result the binding energies $E^\mathrm{y} = 98.35\mathrm{meV}$ (yellow exciton) and $E^\mathrm{g} = 88.46\mathrm{meV}$ (green exciton), and Rydberg energy $E_\mathrm{H} = 13.6\mathrm{eV}$ of the hydrogen atom differ by about two orders of magnitude. Assigning radii a to the binding energies to determine the size of the states yields $a_\mathrm{y} = 0.976\mathrm{nm}$ (yellow exciton) and $a_\mathrm{g} = 1.085\mathrm{nm}$ (green exciton). Thus, the radii of the excitons are about 20 times larger than the Bohr radius $r_0 = 5.29 \times 10^{-11}\mathrm{m}$. Due to the size of the excitons, the sensitivity to external fields also increases. While an electrical permeability $\epsilon_\mathrm{H} = 1$ is assumed in the hydrogen atom, $\epsilon = 7.5$ **[17]** applies to the excitons in Cu_2O.

3.4 Excitons in Cuprous Oxide with Quantum Wells

In order to gain further insights, the current research at the ITP1 is concerned with an additional, spatial restriction of the exciton dynamics by Quantum Wells. The Quantum Well under consideration corresponds to an infinite potential well

$$V = \begin{cases} 0 & \text{, if } |z| < L/2 \\ \infty & \text{, else} \end{cases} \tag{3.6}$$

which is choosen to be along the [001] axis of the crystal. The resulting boundary conditions break the translational symmetry along the z-axis. It should be noted that the condition can be realised experimentally by using a few nanometer thick slice of the sample, so L is typically in the order of nm.

In the case of the hydrogen-like description with Quantum Wells, let the six degrees of freedom $\{x_e, y_e, z_e, x_h, y_h, z_h\}$ be given. Due to the broken translation symmetry, the relative and centre of mass coordinates can only be introduced within the xy-plane. The four degrees of freedom $\{x, y, z_\mathrm{e}, z_\mathrm{h}\}$ remain. A transformation into cylindrical coordinates leads to the four degrees of freedom $\{\rho, \phi, z_\mathrm{e}, z_\mathrm{h}\}$, which can be further reduced to the three degrees of freedom $\{\rho, z_\mathrm{e}, z_\mathrm{h}\}$ by using the remaining rotational symmetry within the xy-plane. A numerical solution of the exciton states for the resulting Hamiltonian (3.2), with additional Quantum Wells $V_\mathrm{e}, V_\mathrm{h}$ has already been dealt with by Pavel Belov [**7**], Leon Kühner [**8**] and currently Niklas Scheuler.

The aim of this bachelor thesis is the analytical reduction of the degrees of freedom of the Hamiltonian containing quantum wells and the band structure, to enable a numerical solution within an adequate computing time.

The Hamiltonian (3.2) with additional Quantum Wells, as introduced in equation (3.6), describe the excitons states in Cu_2O with Quantum Wells. It should be noted that both a Quantum Well for the hole and a Quantum Well for the electron are added. A sketch of the exciton in Cu_2O with Quantum Wells is shown in fig.3.2.

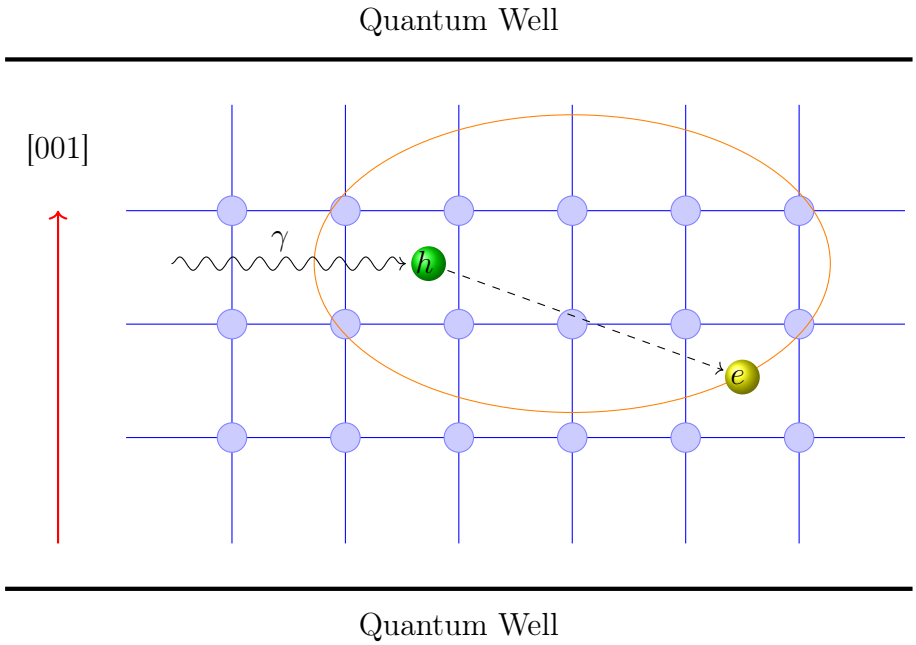

Figure 3.2: Sketch of the bound state of an exciton in a cubic crystal lattice with Quantum Wells along the [001] axis of the crystal.

3.5 Hamiltonian of Excitons in Cuprous Oxide

This section is based on References [**11**, **18**, **19**].

The experimental data from [**5**] show physically determined deviations of the absorption spectrum of the excitons in Cu_2O from that of a hydrogen-like series. A quantum explanation for this is provided by the spin-orbit coupling of the excitons, as well as the interband interactions which together lead to a splitting and deformation of the energy bands. Figure 3.1 shows the splitting of the original Γ_5^+ valence band via the coupling of quasispin $\boldsymbol{I}$ and hole spin $\boldsymbol{S}_\mathrm{h}$ to a doubly degenerate Γ_7^+ and two doubly degenerate Γ_8^+ valence bands. The quasispin

$$\boldsymbol{I}_k = \sum_{l,m} -i\hbar\epsilon_{klm}(\boldsymbol{e}_l \otimes \boldsymbol{e}_m) \tag{3.7}$$

results from the basis vectors $\boldsymbol{e}_l$, $\boldsymbol{e}_m$ and the permutation by the Levi-Civita epsilon tensor ϵ_{klm}. The hole spin $\boldsymbol{S}_\mathrm{h} = \pm\frac{1}{2}$, on the other hand, is only half-odd-integer. We can describe the valence band structure using a form deviating from a parabula. The Suzuki-Hensel Hamiltonian

$$H_{VB}(\boldsymbol{k}) = -H_{\mathrm{SO}} + \frac{1}{2m_0}\Big[\boldsymbol{k}^2(\hbar^2 A_1 + 2B_1 \boldsymbol{I}\boldsymbol{S}_{\mathrm{h}}) + A_2(k_1^2(I_1^2 - \frac{\boldsymbol{I}^2}{3}) + c.p.)$$

$$+B_2(2k_1^2(I_1 S_{\mathrm{h}1} - \frac{\boldsymbol{I}\boldsymbol{S}_{\mathrm{h}}}{3}) + c.p.) + A_3(2\{k_1, k_2\}\{I_1, I_2\} + c.p.) \tag{3.8}$$

$$+B_3(2\{k_1, k_2\}(I_1 S_{\mathrm{h}1} + I_2 S_{\mathrm{h}2}))\Big]$$

from [**19**] is used to represent the band structure and therefore the hole dynamics in the bulk. A_i and B_i with $i \in \{1, 2, 3\}$ correspond to six free parameters. The expression $\{a, b\} = (ab + ba)/2$ serves as an abbreviated notation and

$$H_{\mathrm{SO}} = \frac{2}{3} E_{\mathrm{g}}(1 + \frac{1}{\hbar^2}\boldsymbol{I}\boldsymbol{S}_{\mathrm{h}}) \tag{3.9}$$

with the band gap E_{g} describes the spin-orbit coupling. It is possible to fit the resulting Hamiltonian to a simulation of spin density functional theory or spin DFT [**18**]. With a least square fit, the initially free parameters A_i and B_i result (Tab. 3.2). The definition of the Lutting parameters

$$\begin{aligned} \gamma_1 \equiv -A_1, \gamma_2 \equiv \frac{1}{6}A_2, \gamma_3 \equiv \frac{1}{6}A_3, \\ \eta_1 \equiv -B_1, \eta_2 \equiv \frac{1}{6}B_2, \eta_3 \equiv \frac{1}{6}B_3, \end{aligned} \tag{3.10}$$

allows for a physical interpretation of the parameters. While γ_1 and η_1 correspond to the average effective mass of the hole, the further parameters $\gamma_2, \gamma_3, \eta_2, \eta_3$ stand for the splitting and deformation of the energy bands. It should be said that the conduction band and thus the kinetic energy of the electron, in contrast to the valence band, can still be well regarded as parabolic. This leads to the Hamiltonian of an exciton in Cu_2O. If one now compares the theoretical expectations with the experimental data, the assumption of a non-parabolic band structure is justified. Finally, it should be noted that this derivation of the band structure of Cu_2O can be extended to many other semiconductors. Examples include GaAs and CuBr, where only the values of the parameters differ.

Table 3.2: Parameters A_i and B_i determined by the fit of the Suzuki Hensel Hamiltonian to the band structure of the spin DFT [**18**], as well as the corresponding Luttinger parameters γ_i and η_i.

i	1	2	3	i	1	2	3
A_i	-1.76	4.519	-2.201	γ_i	1.76	0.753	-0.367
B_i	0.02	-0.022	-0.202	η_i	-0.02	-0.004	-0.034

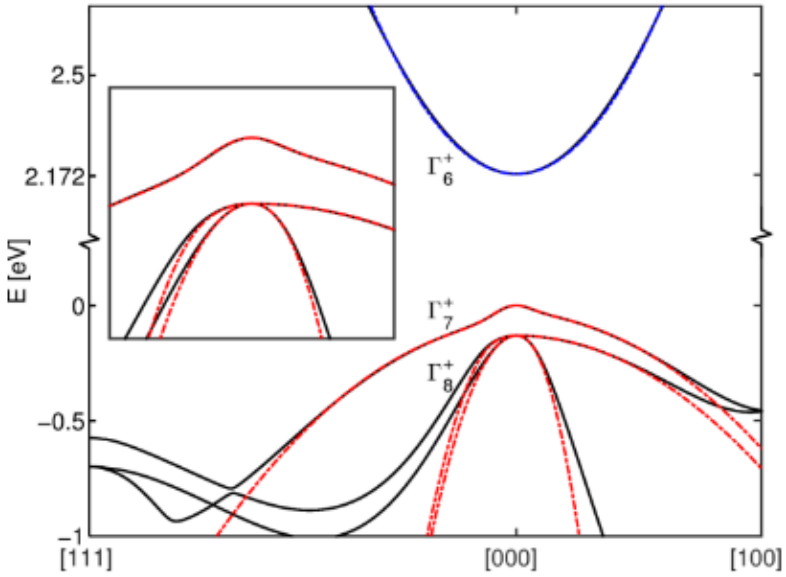

Figure 3.3: Fit of the Suzuki Hensel Hamiltonian to the band structure from the spin DFT. The black lines belong to the band structure of the spin-DFT. The blue line shows the still parabolic lowest conduction band. The red dashed lines show the best fit of the Suzuki Hensel Hamiltonian to the spin DFT and thus determine the values of the free parameters A_i and B_i [**18**].

The Hamiltonian

$$H = E_\mathrm{g} + V + H_\mathrm{e}(\boldsymbol{p}_\mathrm{e}) + H_\mathrm{h}(\boldsymbol{p}_\mathrm{h}) \tag{3.11}$$

to describe excitons in cuprous oxide with Quantum Wells is created by simply adding the infinite potential wells from equation (3.6) to the Hamiltonian (3.2) in the bulk. Now the Suzuki-Hensel Hamiltonian (3.8) with the parameters characteristic for Cu_2O from equation (3.10) describes the dynamics

$$\begin{aligned} H_\mathrm{h}(\boldsymbol{p}_\mathrm{h}) =& H_\mathrm{SO} + \frac{1}{2m_0}(\gamma_1 + 4\gamma_2)\boldsymbol{p}_\mathrm{h}^\mathbf{2} - \frac{3\gamma_2}{\hbar^2 m_0}\sum_{i=1}^{3} p_{\mathrm{hi}}^2 I_i^2 \\ &- \frac{6\gamma_3}{\hbar^2 m_0}(\{p_{h1}, p_{h2}\}\{I_1, I_2\} + \mathrm{c.p.}) \\ &+ \frac{1}{\hbar^2 m_0}(\eta_1 + 2\eta_2)\boldsymbol{I}\boldsymbol{S}_\mathrm{h}\boldsymbol{p}_\mathrm{h}^\mathbf{2} - \frac{6\eta_2}{\hbar^2 m_0}\sum_{i=1}^{3} I_1 S_{\mathrm{h}1} p_{\mathrm{h}1}^2 \\ &- \frac{6\eta_3}{\hbar^2 m_0}\Big(\{p_{\mathrm{h}1}, p_{\mathrm{h}2}\}(I_1 S_{\mathrm{h}2} + I_2 S_{\mathrm{h}1}) + \mathrm{c.p.}\Big) \end{aligned} \tag{3.12}$$

of the hole (h) in the valence band and

$$H_\mathrm{e}(\boldsymbol{p}_\mathrm{e}) = \frac{\boldsymbol{p}_\mathrm{e}^2}{2m_\mathrm{e}} \tag{3.13}$$

describes the dynamics of the electron (e) in the conduction band. H_SO corresponds to the spin-orbit coupling. The potential

$$V = -\frac{1}{4\pi\epsilon_0\epsilon}\frac{1}{|\boldsymbol{r}_\mathrm{e} - \boldsymbol{r}_\mathrm{h}|} + V_\mathrm{e}(z_\mathrm{e}) + V_\mathrm{h}(z_\mathrm{h}) \tag{3.14}$$

contains the Coulomb attraction between electron and hole with the dielectrical constant ϵ_0, the permeability ϵ of Cu_2O as well as the Quantum Wells $V_\mathrm{e}(z_\mathrm{e})$ and $V_\mathrm{h}(z_\mathrm{h})$. Furthermore, $\boldsymbol{r}_\mathrm{e}$ and $\boldsymbol{r}_\mathrm{h}$ correspond to the position operators of electron and hole with the corresponding momentum operators

$$\boldsymbol{p}_{\mathrm{e}} = \frac{\hbar}{i}\Big(\frac{\partial}{\partial x_{\mathrm{e}}}, \frac{\partial}{\partial y_{\mathrm{e}}}, \frac{\partial}{\partial z_{\mathrm{e}}}\Big)^{\mathsf{T}}, \tag{3.15}$$

and

$$\boldsymbol{p}_{\mathrm{h}} = \frac{\hbar}{i}\Big(\frac{\partial}{\partial x_{\mathrm{h}}}, \frac{\partial}{\partial y_{\mathrm{h}}}, \frac{\partial}{\partial z_{\mathrm{h}}}\Big)^{\mathsf{T}} \tag{3.16}$$

including the effective masses $m_{\mathrm{e}} = 0.99 m_0$ and $m_{\mathrm{h}} = m_0/\gamma_1$, and $\hbar$ corresponds to Planck's constant.

4 Cuprous Oxide in Quantum Wells

4.1 Reduction of the Degrees of Freedom of the Hamiltonian

Let the Cu_2O crystal be oriented so that the [001]-axis corresponds to the z-axis. To reduce the degrees of freedom of the Hamiltonian in the bulk, the full three-dimensional translational symmetry was used. The introduction of three-dimensional relative and center of mass coordinates thus makes it possible to reduce the six degrees of freedom $\{x_\mathrm{e}, y_\mathrm{e}, z_\mathrm{e}, x_\mathrm{h}, y_\mathrm{h}, z_\mathrm{h}\}$ to three relative coordinates $\{x, y, z\}$. However, the introduction of Quantum Wells destroys the translational symmetry along the z-axis. As a result, the relative and center of mass coordinates

$$\begin{aligned}(X, Y)^\mathsf{T} = \boldsymbol{R} &= \frac{1}{M}(m_\mathrm{e}(x_\mathrm{e}, y_\mathrm{e})^\mathsf{T} + m_\mathrm{h}(x_\mathrm{h}, y_\mathrm{h})^\mathsf{T}),\\ (x, y)^\mathsf{T} = \boldsymbol{r} &= (x_\mathrm{e}, y_\mathrm{e})^\mathsf{T} - (x_\mathrm{h}, y_\mathrm{h})^\mathsf{T}\end{aligned} \tag{4.1}$$

are introduced only in the xy-plane and the z-components are not altered. Note that $M = m_\mathrm{e} + m_\mathrm{h}$ is the total mass. Thus we define

$$\begin{aligned}\boldsymbol{p} &= (p_1, p_2)^\mathsf{T},\\ \boldsymbol{P} &= (P_1, P_2)^\mathsf{T}\end{aligned} \tag{4.2}$$

as the corresponding, two-dimensional relative and center of mass momenta in the xy-plane. It should be noted that the notation via the indices $\{1, 2\}$ for the momenta in relative and center of mass coordinates on the one hand and holding of the z indices on the other hand, is used to clarify the difference between bulk excitons and excitons in Quantum Wells. In order to express the momentum operators occurring in the Hamiltonian (3.12) by the newly introduced momenta, the chain rule

$$\frac{\partial}{\partial x_j} = \sum_i \frac{\partial x_i}{\partial x_j}\frac{\partial}{\partial x_i}. \tag{4.3}$$

well known from differential calculus is used. If equation (4.3) is evaluated for $x_j \in \{x_\mathrm{e}, y_\mathrm{e}, x_\mathrm{h}, y_\mathrm{h}\}$ and $x_i \in \{x, y, X, Y\}$ then we can find a new expression for the electron and hole momentum

$$\begin{aligned} \boldsymbol{p}_\mathrm{h} &= \begin{pmatrix} p_{\mathrm{h}x} \\ p_{\mathrm{h}y} \\ p_{\mathrm{h}z} \end{pmatrix} = \begin{pmatrix} -p_1 + \frac{m_\mathrm{h}}{M} P_1 \\ -p_2 + \frac{m_\mathrm{h}}{M} P_2 \\ p_\mathrm{hz} \end{pmatrix}, \\ \boldsymbol{p}_\mathrm{e} &= \begin{pmatrix} p_{\mathrm{e}x} \\ p_{\mathrm{e}y} \\ p_{\mathrm{e}z} \end{pmatrix} = \begin{pmatrix} p_1 + \frac{m_\mathrm{e}}{M} P_1 \\ p_2 + \frac{m_\mathrm{e}}{M} P_2 \\ p_\mathrm{ez} \end{pmatrix}. \end{aligned} \tag{4.4}$$

By simply squaring, and applying the commutativity for partial derivatives on the momentum operators, we obtain the quadratic momenta

$$\begin{aligned} \boldsymbol{p}_\mathrm{h}^2 &= \boldsymbol{p}^2 - 2\frac{m_\mathrm{h}}{M}\boldsymbol{p}\boldsymbol{P} + \frac{m_\mathrm{h}^2}{M^2}\boldsymbol{P}^2 + p_\mathrm{hz}^2, \\ \boldsymbol{p}_\mathrm{e}^2 &= \boldsymbol{p}^2 + 2\frac{m_\mathrm{e}}{M}\boldsymbol{p}\boldsymbol{P} + \frac{m_\mathrm{e}^2}{M^2}\boldsymbol{P}^2 + p_\mathrm{ez}^2, \end{aligned} \tag{4.5}$$

occuring in the Hamiltonian and therefore a new expression of the kinetic terms

$$\frac{\boldsymbol{p}_\mathrm{h}^2}{2m_\mathrm{h}} + \frac{\boldsymbol{p}_\mathrm{e}^2}{2m_\mathrm{e}} = \frac{M\boldsymbol{p}^2}{2m_\mathrm{e}m_\mathrm{h}} + \frac{\boldsymbol{P}^2}{2M} + \frac{p_\mathrm{hz}^2}{2m_\mathrm{h}} + \frac{p_\mathrm{ez}^2}{2m_\mathrm{e}}. \tag{4.6}$$

Replace $1/m_\mathrm{h}$ by the effective mass γ_1/m_0 of the hole in the valence band and further identify

$$\frac{\gamma_1'}{m_0} = \frac{\gamma_1}{m_0} + \frac{1}{m_\mathrm{e}} = \frac{M}{m_\mathrm{e}m_\mathrm{h}} \tag{4.7}$$

as the inverse reduced mass. Then equation (4.6) can be expressed as

$$\frac{\boldsymbol{p}_\mathrm{h}^2}{2m_\mathrm{h}} + \frac{\boldsymbol{p}_\mathrm{e}^2}{2m_\mathrm{e}} = \frac{\gamma_1'\boldsymbol{p}^2}{2m_0} + \frac{\boldsymbol{P}^2}{2M} + \frac{p_\mathrm{hz}^2}{2m_\mathrm{h}} + \frac{p_\mathrm{ez}^2}{2m_\mathrm{e}}. \tag{4.8}$$

If we include the results from equation (4.5) and equation (4.8) into the Hamiltonian (3.11), we obtain a representation including relative and center of mass coordinates along the xy-plane.

$$
\begin{aligned}
\boldsymbol{H} =& E_\mathrm{g} + H_\mathrm{SO} + \frac{\gamma_1' \boldsymbol{p}^2}{2m_0} + \frac{\boldsymbol{P}^2}{2M} + \frac{p_\mathrm{hz}^2}{2m_\mathrm{h}} + \frac{p_\mathrm{ez}^2}{2m_\mathrm{e}} \\
& - \frac{1}{4\pi\epsilon_0\epsilon} \frac{1}{\sqrt{\boldsymbol{r}^2 + (z_\mathrm{e} - z_\mathrm{h})^2}} + V_\mathrm{e}(z_\mathrm{e}) + V_\mathrm{h}(z_\mathrm{h}) \\
& + \frac{2\gamma_2}{m_0}\Big[p_1^2 - 2\frac{m_\mathrm{h}}{M} p_1 P_1 + \frac{m_\mathrm{h}^2}{M^2} P_1^2 + p_2^2 - 2\frac{m_\mathrm{h}}{M} p_2 P_2 + \frac{m_\mathrm{h}^2}{M^2} P_2^2 + p_\mathrm{hz}^2\Big] \\
& - \frac{3\gamma_2}{\hbar^2 m_0}\Big[(p_1^2 - 2\frac{m_\mathrm{h}}{M} p_1 P_1 + \frac{m_\mathrm{h}^2}{M^2} P_1^2) I_1^2 \\
& + (p_2^2 - 2\frac{m_\mathrm{h}}{M} p_2 P_2 + \frac{m_\mathrm{h}^2}{M^2} P_2^2) I_2^2 + p_\mathrm{hz}^2 I_3^2\Big] \\
& - \frac{3\gamma_3}{\hbar^2 m_0}\Big[(p_1 p_2 - \frac{m_\mathrm{h}}{M} p_1 P_2 - \frac{m_\mathrm{h}}{M} p_2 P_1 + \frac{m_\mathrm{h}^2}{M^2} P_1 P_2 \\
& + p_2 p_1 - \frac{m_\mathrm{h}}{M} p_2 P_1 - \frac{m_\mathrm{h}}{M} p_1 P_2 + \frac{m_\mathrm{h}^2}{M^2} P_2 P_1)\{I_1, I_2\} \\
& + (-p_2 p_\mathrm{hz} + \frac{m_\mathrm{h}}{M} p_\mathrm{hz} P_2 - p_\mathrm{hz} p_2 + \frac{m_\mathrm{h}}{M} P_2 p_\mathrm{hz})\{I_2, I_3\} \\
& + (-p_\mathrm{hz} p_1 + \frac{m_\mathrm{h}}{M} P_1 p_\mathrm{hz} - p_1 p_\mathrm{hz} + \frac{m_\mathrm{h}}{M} p_\mathrm{hz} P_1)\{I_3, I_1\}\Big] \\
& + \frac{1}{\hbar^2 m_0}(\eta_1 + 2\eta_2)\boldsymbol{I}\boldsymbol{S}_\mathrm{h}\Big[p_1^2 - 2\frac{m_\mathrm{h}}{M} p_1 P_1 + \frac{m_\mathrm{h}^2}{M^2} P_1^2 \\
& + p_2^2 - 2\frac{m_\mathrm{h}}{M} p_2 P_2 + \frac{m_\mathrm{h}^2}{M^2} P_2^2 + p_\mathrm{hz}^2\Big]
\end{aligned}
\tag{4.9}
$$

$$
\begin{aligned}
&- \frac{6\eta_2}{\hbar^2 m_0}\Big[(p_1^2 - 2\frac{m_\mathrm{h}}{M}p_1P_1 + \frac{m_\mathrm{h}^2}{M^2}P_1^2)I_1S_{\mathrm{h}1} \\
&+ (p_2^2 - 2\frac{m_\mathrm{h}}{M}p_2P_2 + \frac{m_\mathrm{h}^2}{M^2}P_2^2)I_2S_{\mathrm{h}2} + p_{\mathrm{hz}}^2 I_3 S_{\mathrm{h}3}\Big] \\
&- \frac{3\eta_3}{\hbar^2 m_0}\Big[(p_1p_2 - \frac{m_\mathrm{h}}{M}p_1P_2 - \frac{m_\mathrm{h}}{M}p_2P_1 + \frac{m_\mathrm{h}^2}{M^2}P_1P_2 \\
&+ p_2p_1 - \frac{m_\mathrm{h}}{M}p_2P_1 - \frac{m_\mathrm{h}}{M}p_1P_2 + \frac{m_\mathrm{h}^2}{M^2}P_2P_1)(I_1S_{\mathrm{h}2} + I_2S_{\mathrm{h}1}) \\
&+ (-p_2p_{\mathrm{hz}} + \frac{m_\mathrm{h}}{M}p_{\mathrm{hz}}P_2 - p_{\mathrm{hz}}p_2 + \frac{m_\mathrm{h}}{M}P_2p_{\mathrm{hz}})(I_2S_{\mathrm{h}3} + I_3S_{\mathrm{h}2}) \\
&+ (-p_{\mathrm{hz}}p_1 + \frac{m_\mathrm{h}}{M}P_1p_{\mathrm{hz}} - p_1p_{\mathrm{hz}} + \frac{m_\mathrm{h}}{M}p_{\mathrm{hz}}P_1)(I_3S_{\mathrm{h}1} + I_1S_{\mathrm{h}3})\Big].
\end{aligned}
$$

Due to the increasing length of the Hamiltonian during the following transformations, it is suitable to divide the Hamiltonian into multiple parts depending on the occuring operators. Beside the dividing, according to the operators $\boldsymbol{p}, \boldsymbol{p}_{\mathrm{hz}}, \boldsymbol{P}$, the Hamiltonian is further subdivided by the occurrence of the parameters γ_i and η_i. The N_i terms include the γ_i parameter and the M_i terms include the η_i parameter. Therefore

$$\sum_i N_i + M_i \tag{4.10}$$

represents the kinetic terms of the Hamiltonian. Also notice that the trivial transformation of the potentials and the constant terms is ignored at first. Thus the separated expressions of the kinetic terms of the Hamiltonian result in

$$N_1(\boldsymbol{p}) = \Big(\frac{\gamma_1'}{2m_0} + \frac{2\gamma_2}{m_0}\Big)\boldsymbol{p^2} - \frac{3\gamma_2}{\hbar^2 m_0}(p_1^2I_1^2 + p_2^2I_2^2) - \frac{6\gamma_3}{\hbar^2 m_0}\Big(\{p_1,p_2\}\{I_1,I_2\}\Big), \tag{4.11}$$

$$N_2(\boldsymbol{p}, p_{\mathrm{hz}}) = \frac{6\gamma_3}{\hbar^2 m_0}\Big(\{p_2,p_{\mathrm{hz}}\}\{I_2,I_3\} + \{p_{\mathrm{hz}},p_1\}\{I_3,I_1\}\Big), \tag{4.12}$$

$$N_3(p_{\mathrm{hz}}) = \Big(\frac{\gamma_1}{2m_0} + \frac{2\gamma_2}{m_0} - \frac{3\gamma_2}{\hbar^2 m_0}I_3^2\Big)p_{\mathrm{hz}}^2, \tag{4.13}$$

$$N_4(p_{\rm hz},\boldsymbol{P}) = -\frac{6\gamma_3 m_{\rm h}}{\hbar^2 m_0 M}\Big(\{P_2,p_{\rm hz}\}\{I_2,I_3\}+\{p_{\rm hz},P_1\}\{I_3,I_1\}\Big), \tag{4.14}$$

$$N_5(\boldsymbol{P}) = \Big(\frac{1}{2M}+\frac{2\gamma_2 m_{\rm h}^2}{m_0 M^2}\Big)\boldsymbol{P^2} - \frac{3\gamma_2 m_{\rm h}^2}{\hbar^2 m_0 M^2}(P_1^2 I_1^2 + P_2^2 I_2^2), \tag{4.15}$$

$$N_6(\boldsymbol{p},\boldsymbol{P}) = -\frac{4\gamma_2 m_{\rm h}}{m_0 M}(p_1P_1+p_2P_2) + \frac{6\gamma_2 m_{\rm h}}{\hbar^2 m_0 M}(p_1P_1I_1^2+p_2P_2I_2^2), \tag{4.16}$$

$$N_7(p_{\rm ez}) = \frac{1}{2m_{\rm e}}p_{\rm ez}^2, \tag{4.17}$$

$$\begin{aligned} M_1(\boldsymbol{p}) =& \frac{1}{\hbar^2 m_0}(\eta_1+2\eta_2)(\boldsymbol{I}\cdot\boldsymbol{S}_{\rm h})\boldsymbol{p^2} - \frac{6\eta_2}{\hbar^2 m_0}(p_1^2 I_1 S_{\rm h1} + p_2^2 I_2 S_{\rm h2}) \\ & - \frac{6\eta_3}{\hbar^2 m_0}\Big(\{p_1,p_2\}(I_1S_{\rm h2}+I_2S_{\rm h1})\Big), \end{aligned} \tag{4.18}$$

$$M_2(\boldsymbol{p},p_{\rm hz}) = \frac{6\eta_3}{\hbar^2 m_0}\Big(\{p_2,p_{\rm hz}\}(I_2S_{\rm h3}+I_3S_{\rm h2})+\{p_{\rm hz},p_1\}(I_3S_{\rm h1}+I_1S_{\rm h3})\Big), \tag{4.19}$$

$$M_3(p_{\rm hz}) = \Big(\frac{1}{\hbar^2 m_0}(\eta_1+2\eta_2)(\boldsymbol{I}\cdot\boldsymbol{S}_{\rm h}) - \frac{6\eta_2}{\hbar^2 m_0}I_3S_{\rm h3}\Big)p_{\rm hz}^2, \tag{4.20}$$

$$\begin{aligned} M_4(p_{\rm hz},\boldsymbol{P}) =& -\frac{6\eta_3 m_{\rm h}}{\hbar^2 m_0 M}\Big(\{P_2,p_{\rm hz}\}(I_2S_{\rm h3}+I_3S_{\rm h2}) \\ & + \{p_{\rm hz},P_1\}(I_3S_{\rm h1}+I_1S_{\rm h3})\Big), \end{aligned} \tag{4.21}$$

$$\begin{aligned} M_5(\boldsymbol{P}) =& \frac{m_{\rm h}^2}{\hbar^2 m_0 M^2}(\eta_1+2\eta_2)(\boldsymbol{I}\cdot\boldsymbol{S}_{\rm h})\boldsymbol{P^2} - \frac{6\eta_2 m_{\rm h}^2}{\hbar^2 m_0 M^2}(P_1^2 I_1 S_{\rm h1} + P_2^2 I_2 S_{\rm h2}) \\ & - \frac{6\eta_3 m_{\rm h}^2}{\hbar^2 m_0 M^2}\{P_1,P_2\}(I_1S_{\rm h2}+I_2S_{\rm h1}), \end{aligned} \tag{4.22}$$

and

$$
\begin{aligned}
M_6(\boldsymbol{p},\boldsymbol{P}) = &-\frac{2m_\mathrm{h}}{\hbar^2 m_0 M}(\eta_1+2\eta_2)(\boldsymbol{I}\cdot\boldsymbol{S}_\mathrm{h})(p_1P_1+p_2P_2)\\
&+\frac{12\eta_2 m_\mathrm{h}}{\hbar^2 m_0 M}(p_1P_1I_1S_{\mathrm{h}1}+p_2P_2I_2S_{\mathrm{h}2})\\
&+\frac{6\eta_3 m_\mathrm{h}}{\hbar^2 m_0 M}(p_1P_2+p_2P_1)(I_1S_{\mathrm{h}2}+I_2S_{\mathrm{h}1}).
\end{aligned}
\tag{4.23}
$$

Now we want to use the introduced center of mass coordinates and the associated two-dimensional translation symmetry. For this, the center of mass frame is chosen as the reference frame. In the center of mass frame $\boldsymbol{P}=0$ is valid and thus all $\boldsymbol{P}$ dependent N_i and M_i terms disappear, which corresponds to an enormous reduction of the Hamiltonian to

$$
\begin{aligned}
\boldsymbol{H} =&E_\mathrm{g}+H_\mathrm{SO}-\frac{1}{4\pi\epsilon_0\epsilon}\frac{1}{\sqrt{\boldsymbol{r}^2+(z_\mathrm{e}-z_\mathrm{h})^2}}+V_\mathrm{e}(z_\mathrm{e})+V_\mathrm{h}(z_\mathrm{h})\\
&+\Big(\frac{\gamma_1'}{2m_0}+\frac{2\gamma_2}{m_0}\Big)\boldsymbol{p}^2-\frac{3\gamma_2}{\hbar^2 m_0}(p_1^2I_1^2+p_2^2I_2^2)-\frac{6\gamma_3}{\hbar^2 m_0}\Big(\{p_1,p_2\}\{I_1,I_2\}\Big)\\
&+\frac{6\gamma_3}{\hbar^2 m_0}\Big(\{p_2,p_\mathrm{hz}\}\{I_2,I_3\}+\{p_\mathrm{hz},p_1\}\{I_3,I_1\}\Big)\\
&+\frac{1}{\hbar^2 m_0}(\eta_1+2\eta_2)(\boldsymbol{I}\cdot\boldsymbol{S}_\mathrm{h})\boldsymbol{p}^2-\frac{6\eta_2}{\hbar^2 m_0}(p_1^2I_1S_{\mathrm{h}1}+p_2^2I_2S_{\mathrm{h}2})\\
&-\frac{6\eta_3}{\hbar^2 m_0}\Big(\{p_1,p_2\}(I_1S_{\mathrm{h}2}+I_2S_{\mathrm{h}1})\Big)\\
&+\frac{6\eta_3}{\hbar^2 m_0}\Big(\{p_2,p_\mathrm{hz}\}(I_2S_{\mathrm{h}3}+I_3S_{\mathrm{h}2})+\{p_\mathrm{hz},p_1\}(I_3S_{\mathrm{h}1}+I_1S_{\mathrm{h}3})\Big)\\
&+\Big(\frac{1}{\hbar^2 m_0}(\eta_1+2\eta_2)(\boldsymbol{I}\cdot\boldsymbol{S}_\mathrm{h})-\frac{6\eta_2}{\hbar^2 m_0}I_3S_{\mathrm{h}3}+\frac{\gamma_1}{2m_0}+\frac{2\gamma_2}{m_0}-\frac{3\gamma_2}{\hbar^2 m_0}I_3^2\Big)p_\mathrm{hz}^2.
\end{aligned}
\tag{4.24}
$$

It should also be noted that the six degrees of freedom $\{x, y, z_\mathrm{e}, z_\mathrm{h}, X, Y\}$ of the Hamiltonian are thus reduced to the four degrees of freedom $\{x, y, z_\mathrm{e}, z_\mathrm{h}\}$. Compared to the excitons in bulk, the introduction of Quantum Wells thus lead to an additional degree of freedom. If the exciton is described as hydrogen-like, again the degrees of freedom of the Hamiltonian can be further reduced by exploiting the rotational symmetry in the xy-plane. However, the additionally considered band structure destroys the full rotational symmetry, and therefore the degrees of freedom cannot be further reduced. Since the programme known to us for solving the exciton states was implemented for the hydrogen-like exciton, and therefore also in cylindrical coordinates, we will nevertheless carry out a further transformation into cylindrical coordinates. Note that here we again fix the z-components and perform the transformation only for the relative coordinates in the xy-plane. A transformation of the two relative coordinates into plane polar coordinates thus corresponds to a transformation of the Hamiltonian into cylindrical coordinates. This transformation is well known and we choose

$$x = \rho \cos\phi, \tag{4.25}$$

and

$$y = \rho \sin\phi, \tag{4.26}$$

with $\phi \in [0, 2\pi)$. In order to represent the momentum operators in plane polar coordinates, the corresponding set of partial derivatives

$$\Big(\frac{\partial^2}{\partial x^2}, \frac{\partial^2}{\partial y^2}, \frac{\partial}{\partial x}\frac{\partial}{\partial y}, \frac{\partial}{\partial x}, \frac{\partial}{\partial y}\Big), \tag{4.27}$$

are first represented in the generating set

$$\Big(\frac{\partial^2}{\partial \rho^2}, \frac{\partial^2}{\partial \phi^2}, \frac{\partial}{\partial \rho}\frac{\partial}{\partial \phi}, \frac{\partial}{\partial \rho}, \frac{\partial}{\partial \phi}\Big). \tag{4.28}$$

Using the chain rule from equation (4.3) again, we obtain the representations

$$\frac{\partial}{\partial x} = \cos\phi \frac{\partial}{\partial \rho} - \frac{\sin\phi}{\rho}\frac{\partial}{\partial \phi}, \tag{4.29}$$

$$\frac{\partial}{\partial y} = \sin\phi \frac{\partial}{\partial \rho} + \frac{\cos\phi}{\rho}\frac{\partial}{\partial \phi}, \tag{4.30}$$

$$\frac{\partial^2}{\partial x^2} = \cos^2\phi\frac{\partial^2}{\partial\rho^2} + \frac{2\cos\phi\sin\phi}{\rho^2}\left[\frac{\partial}{\partial\phi} - \rho\frac{\partial}{\partial\rho}\frac{\partial}{\partial\phi}\right] + \frac{\sin^2\phi}{\rho^2}\left[\rho\frac{\partial}{\partial\rho} + \frac{\partial^2}{\partial\phi^2}\right], \tag{4.31}$$

$$\frac{\partial^2}{\partial y^2} = \sin^2\phi\frac{\partial^2}{\partial\rho^2} - \frac{2\sin\phi\cos\phi}{\rho^2}\left[\frac{\partial}{\partial\phi} - \rho\frac{\partial}{\partial\rho}\frac{\partial}{\partial\phi}\right] + \frac{\cos^2\phi}{\rho^2}\left[\rho\frac{\partial}{\partial\rho} + \frac{\partial^2}{\partial\phi^2}\right], \tag{4.32}$$

and

$$\frac{\partial}{\partial y}\frac{\partial}{\partial x} = \frac{\sin\phi\cos\phi}{\rho^2}\left[\rho^2\frac{\partial^2}{\partial\rho^2} - \rho\frac{\partial}{\partial\rho} - \frac{\partial^2}{\partial\phi^2}\right] + \frac{\cos^2\phi - \sin^2\phi}{\rho^2}\left[-\frac{\partial}{\partial\phi} + \rho\frac{\partial}{\partial\rho}\frac{\partial}{\partial\phi}\right]. \tag{4.33}$$

Note that taking into account the definition range of the required inverse functions and a case distinction, the same partial derivatives follow in all quadrants. Also a more detailed calculation for the determination of the derivatives can be found in the appendix A.2. With the obtained representations of the partial derivatives, the transformation into plane polar coordinates can be carried out via matrix multiplication with the transition matrix $M_{5\times5}$. This method was chosen because it turned out to be the clearest for me personally. The columns of the transition matrix

$$M_{5\times5} = \begin{bmatrix} c^2 & s^2 & sc & 0 & 0 \\ \frac{s^2}{\rho^2} & \frac{c^2}{\rho^2} & -\frac{sc}{\rho^2} & 0 & 0 \\ -\frac{2sc}{\rho} & \frac{2sc}{\rho} & \frac{c^2-s^2}{\rho} & 0 & 0 \\ \frac{s^2}{\rho} & \frac{c^2}{\rho} & -\frac{sc}{\rho} & c & s \\ \frac{2sc}{\rho^2} & -\frac{2sc}{\rho^2} & \frac{s^2-c^2}{\rho^2} & -\frac{s}{\rho} & \frac{c}{\rho} \end{bmatrix}$$

from left to right correspond to the partial derivatives from equation (4.27), from left to right. The rows from top to bottom correspond to the partial derivatives from equation (4.28), also from left to right. The entries of the transition matrix are the corresponding prefactors of the equations (4.29) to (4.33). The M_{11} component thus corresponds, for example, to the prefactor of the twofold partial derivative with respect to ρ in equation (4.31). It should be noted that the abbreviations $s := \sin\phi$, and $c := \cos\phi$ were also used within the transiton matrix for better representability. The representation of the Hamiltonian in cylindrical coordinates is done via the generating set from equation (4.28), with the corresponding coefficients. The searched coefficients are determined via the transition matrix. Let the row vector be

$$A_{5\times1} = (A_{\mathrm{xx}}, A_{\mathrm{yy}}, A_{\mathrm{xy}}, A_{\mathrm{x}}, A_{\mathrm{y}})^{\mathsf{T}} \tag{4.34}$$

with entries

$$A_{\mathrm{xx}} = -\frac{\hbar^2}{2m_0}(\gamma_1' + 4\gamma_2) + \frac{3\gamma_2}{m_0}I_1^2 - \frac{\boldsymbol{IS}_{\mathrm{h}}}{m_0}(\eta_1 + 2\eta_2) + \frac{6\eta_2}{m_0}I_1 S_{\mathrm{h1}}, \tag{4.35}$$

$$A_{\mathrm{yy}} = -\frac{\hbar^2}{2m_0}(\gamma_1' + 4\gamma_2) + \frac{3\gamma_2}{m_0}I_2^2 - \frac{\boldsymbol{IS}_{\mathrm{h}}}{m_0}(\eta_1 + 2\eta_2) + \frac{6\eta_2}{m_0}I_2 S_{\mathrm{h2}}, \tag{4.36}$$

$$A_{\mathrm{xy}} = \frac{6\gamma_3}{m_0}\{I_1, I_2\} + \frac{6\eta_3}{m_0}(I_1 S_{\mathrm{h2}} + I_2 S_{\mathrm{h1}}), \tag{4.37}$$

$$A_{\mathrm{x}} = -\frac{6i\gamma_3}{m_0}p_{\mathrm{hz}}\{I_3, I_1\} - \frac{6i\eta_3}{m_0}p_{\mathrm{hz}}(I_3 S_{\mathrm{h1}} + I_1 S_{\mathrm{h3}}), \tag{4.38}$$

$$A_{\mathrm{y}} = -\frac{6i\gamma_3}{m_0}p_{\mathrm{hz}}\{I_2, I_3\} - \frac{6i\eta_3}{m_0}p_{\mathrm{hz}}(I_2 S_{\mathrm{h3}} + I_3 S_{\mathrm{h2}}) \tag{4.39}$$

given, which contains the coefficients of the partial derivatives in the relative coordinates. If the transition matrix is multiplied from the left to the row vector $A'_{5\times1} = M_{5\times5}A_{5\times1}$, then the resulting row vector reads

$$A'_{5\times1} = (A_{\rho\rho}, A_{\phi\phi}, A_{\rho\phi}, A_{\rho}, A_{\phi})^{\mathsf{T}} \tag{4.40}$$

with the entries

$$\begin{aligned} A_{\rho\rho} = &-\frac{\hbar^2}{2m_0}(\gamma_1' + 4\gamma_2) + \frac{3\gamma_2}{m_0}(I_1^2\cos^2\phi + I_2^2\sin^2\phi) \\ &- \frac{\boldsymbol{IS}_{\mathrm{h}}}{m_0}(\eta_1 + 2\eta_2) + \frac{6\eta_2}{m_0}(I_1 S_{\mathrm{h1}}\cos^2\phi + I_2 S_{\mathrm{h2}}\sin^2\phi) \\ &+ \frac{6}{m_0}\sin\phi\cos\phi(\gamma_3\{I_1, I_2\} + \eta_3(I_1 S_{\mathrm{h2}} + I_2 S_{\mathrm{h1}})), \end{aligned} \tag{4.41}$$

$$\begin{aligned}
\rho^2 A_{\phi\phi} =& -\frac{\hbar^2}{2m_0}(\gamma_1' + 4\gamma_2) + \frac{3\gamma_2}{m_0}(I_1^2 \sin^2\phi + I_2^2 \cos^2\phi) \\
&- \frac{\boldsymbol{I}\boldsymbol{S}_\mathrm{h}}{m_0}(\eta_1 + 2\eta_2) + \frac{6\eta_2}{m_0}(I_1 S_\mathrm{h1} \sin^2\phi + I_2 S_\mathrm{h2} \cos^2\phi) \\
&+ \frac{6}{m_0}\sin\phi\cos\phi(\gamma_3\{I_1, I_2\} + \eta_3(I_1 S_\mathrm{h2} + I_2 S_\mathrm{h1})),
\end{aligned} \tag{4.42}$$

$$\begin{aligned}
\rho A_{\rho\phi} =& \frac{6}{m_0}(-\sin\phi\cos\phi(\gamma_2(I_1^2 - I_2^2) + 2\eta_2(I_1 S_\mathrm{h1} - I_2 S_\mathrm{h2})) \\
&+ (\cos^2\phi - \sin^2\phi)(\gamma_3\{I_1, I_2\} + \eta_3(I_1 S_\mathrm{h2} + I_2 S_\mathrm{h1}))),
\end{aligned} \tag{4.43}$$

$$\begin{aligned}
A_\rho =& \frac{1}{\rho}\Big[-\frac{\hbar^2}{2m_0}(\gamma_1' + 4\gamma_2) + \frac{3\gamma_2}{m_0}(I_1^2 \sin^2\phi + I_2^2 \cos^2\phi) - \frac{\boldsymbol{I}\boldsymbol{S}_\mathrm{h}}{m_0}(\eta_1 + 2\eta_2) \\
&+ \frac{6\eta_2}{m_0}(I_1 S_\mathrm{h1} \cos^2\phi + I_2 S_\mathrm{h2} \sin^2\phi - \frac{6}{m_0}\sin\phi\cos\phi(\gamma_3\{I_1, I_2\} \\
&+ \eta_3(I_1 S_\mathrm{h2} + I_2 S_\mathrm{h1}))\Big] - p_\mathrm{hz}\Big[\frac{6i}{\hbar m_0}(\cos\phi(\gamma_3\{I_3, I_1\} + \eta_3(I_3 S_\mathrm{h1} + I_1 S_\mathrm{h3})) \\
&+ \sin\phi(\gamma_3\{I_2, I_3\} + \eta_3(I_2 S_\mathrm{h3} + I_3 S_\mathrm{h2}))\Big],
\end{aligned} \tag{4.44}$$

$$\begin{aligned}
A_\phi =& \frac{1}{\rho^2}\Big[\frac{6}{m_0}\sin\phi\cos\phi(\gamma_2(I_1^2 - I_2^2) - 2\eta_2(I_1 S_\mathrm{h1} - I_2 S_\mathrm{h2})) \\
&- \frac{6}{m_0}(\cos^2\phi - \sin^2\phi)(\gamma_3\{I_1, I_2\} + \eta_3(I_1 S_\mathrm{h2} + I_2 S_\mathrm{h1}))\Big] \\
&- \frac{p_\mathrm{hz}}{\rho}\Big[\frac{6i}{\hbar m_0}\cos\phi(\gamma_3\{I_2, I_3\} + \eta_3(I_2 S_\mathrm{h3} + I_3 S_\mathrm{h2})) \\
&- \sin\phi((\gamma_3\{I_3, I_1\} + \eta_3(I_3 S_\mathrm{h1} + I_1 S_\mathrm{h3}))\Big].
\end{aligned} \tag{4.45}$$

The entries correspond to the new coefficients of the partial derivatives in cylindrical coordinates. Notice that the relation

$$p_\alpha = -i\hbar\partial_\alpha \tag{4.46}$$

has already been used. To further reduce the length of the hamiltonian we use the well known trigonometric identities

$$\sin 2\phi = 2\sin\phi\cos\phi, \tag{4.47}$$

and

$$\cos 2\phi = \cos^2\phi - \sin^2\phi. \tag{4.48}$$

By rearranging the Hamiltonian in respect to the remaining degrees of freedom and their corresponding momentum operators, and also including the previously omitted terms

$$E_\mathrm{g} + H_\mathrm{SO} - \frac{1}{4\pi\epsilon_0\epsilon}\frac{1}{\sqrt{\rho^2 + (z_\mathrm{e} - z_\mathrm{h})^2}} + V_\mathrm{e}(z_\mathrm{e}) + V_\mathrm{h}(z_\mathrm{h}) \tag{4.49}$$

we obtain the Hamiltonian $H(\rho, \phi, p_\rho, p_\phi, z_\mathrm{h}, z_\mathrm{e}, p_\mathrm{hz}, p_\mathrm{ez}, \boldsymbol{I}, \boldsymbol{S}_\mathrm{h})$ for the exciton in the bulk and with Quantum Wells along the [001]-axis of the crystal. Compared to the description in the bulk, as well as to the hydrogen-like description with Quantum Wells, an additional degree of freedom is preserved. Also included are the six spin degrees of freedom $\boldsymbol{I}, \boldsymbol{S}_\mathrm{h}$ resulting from the band structure. Written out, the Hamiltonian results in

$$\begin{aligned} H =& E_\mathrm{g} + H_\mathrm{SO} - \frac{1}{4\pi\epsilon_0\epsilon}\frac{1}{\sqrt{\rho^2 + (z_\mathrm{e} - z_\mathrm{h})^2}} + V_\mathrm{e}(z_\mathrm{e}) + V_\mathrm{h}(z_\mathrm{h}) \\ &+ \frac{1}{2\hbar^2 m_0}\Big[\hbar^2(\gamma_1 + 4\gamma_2) - 6\gamma_2 I_3^2 + 2\boldsymbol{I}\boldsymbol{S}_\mathrm{h}(\eta_1 + 2\eta_2) - 12 I_3 S_\mathrm{h3}\Big]p_\mathrm{hz}^2 + \frac{1}{2m_\mathrm{e}}p_\mathrm{ez}^2 \\ &+ \frac{i}{2\hbar m_0}\Big[-\hbar^2(\gamma_1' + 4\gamma_2) - 2\boldsymbol{I}\boldsymbol{S}_\mathrm{h}(\eta_1 + 2\eta_2) + 6\gamma_2(I_1^2\sin^2\phi + I_2^2\cos^2\phi) \end{aligned} \tag{4.50}$$

$$+ 12\eta_2(I_1 S_{\mathrm{h}1}\sin^2\phi + I_2 S_{\mathrm{h}2}\cos^2\phi) - 6\sin 2\phi(\gamma_3\{I_1, I_2\} + \eta_3(I_1 S_{\mathrm{h}2} + I_2 S_{\mathrm{h}1}))\Big]\frac{1}{\rho}p_\rho$$

$$+ \frac{6}{\hbar^2 m_0}\Big[\cos\phi(\gamma_3\{I_3, I_1\} + \eta_3(I_3 S_{\mathrm{h}1} + I_1 S_{\mathrm{h}3})$$

$$+ \sin\phi(\gamma_3\{I_2, I_3\} + \eta_3(I_2 S_{\mathrm{h}3} + I_3 S_{\mathrm{h}2}))\Big]p_{\mathrm{hz}}p_\rho$$

$$+ \frac{3i}{\hbar m_0}\Big[\sin 2\phi(\gamma_2(I_1^2 - I_2^2) + 2\eta_2(I_1 S_{\mathrm{h}1} - I_2 S_{\mathrm{h}2}))$$

$$- 2\cos 2\phi(\gamma_3\{I_1, I_2\} + \eta_3(I_1 S_{\mathrm{h}2} + I_2 S_{\mathrm{h}1}))\Big]\frac{1}{\rho^2}p_\phi$$

$$+ \frac{6}{\hbar^2 m_0}\Big[\cos\phi(\gamma_3\{I_2, I_3\} + \eta_3(I_2 S_{\mathrm{h}3} + I_3 S_{\mathrm{h}2}))$$

$$- \sin\phi(\gamma_3\{I_3, I_1\} + \eta_3(I_3 S_{\mathrm{h}1} + I_1 S_{\mathrm{h}3}))\Big]\frac{p_{\mathrm{hz}}}{\rho}p_\phi$$

$$+ \frac{1}{2\hbar^2 m_0}\Big[\hbar^2(\gamma_1' + 4\gamma_2) + 2\boldsymbol{I}\boldsymbol{S}_{\mathrm{h}}(\eta_1 + 2\eta_2) - 6\gamma_2(I_1^2\cos^2\phi + I_2^2\sin^2\phi)$$

$$- 12\eta_2(I_1 S_{\mathrm{h}1}\cos^2\phi + I_2 S_{\mathrm{h}2}\sin^2\phi) - 6\sin 2\phi(\gamma_3\{I_1, I_2\} + \eta_3(I_1 S_{\mathrm{h}2} + I_2 S_{\mathrm{h}1}))\Big]p_\rho^2$$

$$+ \frac{1}{2\hbar^2 m_0}\Big[\hbar^2(\gamma_1' + 4\gamma_2) + 2\boldsymbol{I}\boldsymbol{S}_{\mathrm{h}}(\eta_1 + 2\eta_2) - 6\gamma_2(I_1^2\sin^2\phi + I_2^2\cos^2\phi)$$

$$- 12\eta_2(I_1 S_{\mathrm{h}1}\sin^2\phi + I_2 S_{\mathrm{h}2}\cos^2\phi) + 6\sin 2\phi(\gamma_3\{I_1, I_2\} + \eta_3(I_1 S_{\mathrm{h}2} + I_2 S_{\mathrm{h}1}))\Big]\frac{1}{\rho^2}p_\phi^2$$

$$+ \frac{3}{\hbar^2 m_0}\Big[\sin 2\phi(\gamma_2(I_1^2 - I_2^2) + 2\eta_2(I_1 S_{\mathrm{h}1} - I_2 S_{\mathrm{h}2}))$$

$$- 2\cos 2\phi(\gamma_3\{I_1, I_2\} + \eta_3(I_1 S_{\mathrm{h}2} + I_2 S_{\mathrm{h}1}))\Big]\frac{1}{\rho}p_\rho p_\phi.$$

4.2 Discussion

4.2.1 Discrete Rotational Symmetry

To check the obtained Hamiltonian, a test for the discrete rotational symmetry (C_4) of the crystal is carried out in the following. It should be noted that due to the quantum wells along the z-axis, the full $3C_4$ rotational symmetry does not exist and therefore the rotation is only performed in the (x, y)-plane. The transformation

$$\begin{aligned}(\phi, \rho) \rightarrow &(\phi' - \frac{\pi}{2}, \rho') \\ (\frac{\partial}{\partial\phi}, \frac{\partial}{\partial\rho}) \rightarrow &(\frac{\partial}{\partial\phi'}, \frac{\partial}{\partial\rho'})\end{aligned} \tag{4.51}$$

is used. This transformation also affects hole and quasispin

$$(x, y, I_1, I_2, S_{\mathrm{h1}}, S_{\mathrm{h2}}) \rightarrow (y', -x', I_2, -I_1, S_{\mathrm{h2}}, -S_{\mathrm{h1}}) \tag{4.52}$$

and with the known relations of the trigonometric functions

$$\begin{aligned}\sin\phi' + \frac{\pi}{2} &= \cos\phi' \\ \cos\phi' + \frac{\pi}{2} &= -\sin\phi',\end{aligned} \tag{4.53}$$

the transformed Hamitlonian (A.4), shown in the appendix results. The different prefactos of all combinations of momenta remain invariant as if ϕ had been replaced by ϕ' and ρ by ρ'. Thus the invariance with respect to the discrete $\pi/2$ rotation was shown.

4.2.2 Good Quantum Numbers and Outlook for Numerical Solution

In general, the energy eigenvalues of the Hamiltonian are of particular interest. Using the bracket notation, the stationary Schrödinger equation

$$H|\psi\rangle = E|\psi\rangle \tag{4.54}$$

has to be solved. Let $|b_i\rangle$ be the basis of the Hilbert space for square-integrable functions, then the representation

$$|\psi\rangle = \sum_i c_i |b_i\rangle \tag{4.55}$$

results. By multiplying $\langle b_j|$ from the left to equation (4.54) we obtain

$$\begin{aligned} \langle b_j|H|\psi\rangle =& E\langle b_j|\psi\rangle \\ \Leftrightarrow \sum_i \langle b_j|H|b_i\rangle c_i =& E\sum_i c_i \langle b_j|b_i\rangle. \end{aligned} \tag{4.56}$$

Since the basis $|\phi_i\rangle$ is not an orthonormal basis in general, the general eigenvalue equation

$$\sum_i H_{ji} c_i = E \sum_i M_{ji} c_i \tag{4.57}$$

is obtained with the overlap matrix M_{ji}. In order to determine the components H_{ij} of the Hamiltonian, the basis vectors $|\phi_i\rangle$ are needed. For this purpose, consider the degrees of freedom $\{\rho, \phi, z_\mathrm{e}, z_\mathrm{h}\}$ and the spins $\{\boldsymbol{I}, \mathbf{S}_\mathrm{h}\}$ of the Hamiltonian (4.50). The wave function

$$\psi(\rho, \phi, z_\mathrm{e}, z_\mathrm{h}, \boldsymbol{I}, \mathbf{S}_\mathrm{h}) = \sum_i c_i b_i(\rho, \phi, z_\mathrm{e}, z_\mathrm{h}, \boldsymbol{I}, \mathbf{S}_\mathrm{h}) \tag{4.58}$$

can now be developed via a corresponding basis. However, the effective spin $\boldsymbol{J} = \boldsymbol{I} + \boldsymbol{S}_\mathrm{h}$ and its projection $\boldsymbol{M}_J$ are used to replace spin S_h and quasispin I and we rewrite

$$\psi(\rho, \phi, z_\mathrm{e}, z_\mathrm{h}, \boldsymbol{J}, M_\mathrm{J}) = \sum_i c_i b_i(\rho, \phi, z_\mathrm{e}, z_\mathrm{h}, \boldsymbol{J}, M_\mathrm{J}). \tag{4.59}$$

For the approach to represent $|b_i\rangle$ choose

$$\begin{aligned} |b_i\rangle = & \sum_{N_\rho, N_{z_e}, N_{z_h}, M_L, \boldsymbol{J}, M_J} C_{N_\rho, N_{z_e}, N_{z_h}, M_L, \boldsymbol{J}, M_J} \\ & \exp\{iM_l\phi\} B_{N_\rho}(\rho) B_{N_{z_e}}(z_e) B_{N_{z_h}}(z_h) \, |\boldsymbol{J}, M_J\rangle \end{aligned} \tag{4.60}$$

with the B-spline functions $B_{N_\rho}(\rho), B_{N_{z_e}}(z_e), B_{N_{z_h}}(z_h)$ [**8**] and the projection M_L of the angular momentum

$$M_L = -i\hbar\frac{\partial}{\partial\phi}. \tag{4.61}$$

With the help of the chosen basis, the entries of the Hamiltonian can be determined. The Hamiltonian, which corresponds to an infinite-dimensional operator in theory, cannot be realised practically, of course. In practice, the Hamiltonian operator is therefore represented by a large but finite matrix, which describes the Hamiltonian with a negligible error.

It should be noted that this approach to diagonalise the Hamiltonian by using B-spline functions was re-motivated by the preliminary work of Pavel Belov [**7**] and Leon Kühner [**8**].

5 Summary and Outlook

5.1 English Summary

Excitons, postulated in the 1930s, play an important role in the fundamental research of optical properties of semiconductors and insulators. While previous research at ITP1 has mainly focused on excitons in the bulk, this bachelor thesis deals with an additional spatial boundary of the crystal, the Quantum Wells.

The bound states of electron and hole can be described as hydrogen-like in a first approximation. An already implemented programme serves as a numerical solution approach for the hydrogen-like description, containing Quantum Wells.

For a more detailed description of the exciton states, however, the crystal structure must also be taken into account. As a known approach to consider the band structure of Cu_2O, the Suzuki-Hensel-Hamiltonian is chosen. The free parameters are determined by a fit of the Hamiltonian to a simulation of the spin DFT. Since the naive diagonalisation of the resulting Hamiltonian with the already known programme would not provide adequate computing time, both the programme and the Hamiltonian must first be modified. The numerical optimisation is applied simultaneously in another bachelor thesis at the ITP1.

This bachelor thesis, on the other hand, deals with an analytical consideration of the Hamiltonian. The aim is to reduce the degrees of freedom of the Hamiltonian by using the given symmetries, and thus to minimise the required computing time for the diagonalisation.

The starting point of the bachelor thesis is the Hamiltonian dependent on the twelve degrees of freedom $\{x_\mathrm{e}, y_\mathrm{e}, z_\mathrm{e}, x_\mathrm{h}, y_\mathrm{h}, z_\mathrm{h}, I, S_\mathrm{h}\}$, in three-dimensional cartesian coordinates. Although the translational symmetry along the z-axis is destroyed by the introduced Quantum Wells, it is still preserved within the xy-plane. By introducing two-dimensional relative and center of mass coordinates within the xy-plane, the twelve degrees of freedom $\{x, y, X, Y, z_\mathrm{e}, z_\mathrm{h}, I, S_\mathrm{h}\}$ result. The choice of the center of mass frame, as the reference frame, with $P_X = P_Y = 0$ reduces the system to ten degrees of freedom $\{x, y, z_\mathrm{e}, z_\mathrm{h}, I, S_\mathrm{h}\}$.

In the case of the hydrogen-like description, the degrees of freedom could be further reduced by taking advantage of the rotational symmetry within the xy-plane. However, this continuous symmetry is broken down to a four-fold discrete symmetry by the band structure. As a consequence, the ϕ dependence of the Hamiltonian is preserved during the transformation into cylindrical coordinates. The transformation is nevertheless carried out because of later advantages in the numerical solution. Finally, ten degrees of freedom $\{\rho, \phi, z_\mathrm{e}, z_\mathrm{h}, I, S_\mathrm{h}\}$ result.

The calculation was controlled both via a test of the discrete rotational symmetry and via Mathematica. As an outlook, a suitable basis for the diagionalisation of the Hamiltonian was outlined, whereby the choice of the B-spline functions is motivated by a previous bachelor thesis. In the future, this should enable the numerical solution of the exciton states with consideration of the band structure, and the spatial restriction by Quantum Wells.

5.2 German Summary

Die in den 1930er Jahren postulierten Exzitonen spielen eine bedeutende Rolle in der Grundlagenforschung optischer Eigenschaften von Halbleitern und Isolatoren. Während sich die bisherige Forschung am ITP1 hauptsächlich auf Exzitonen im Bulk konzentrierte, beschäftigt sich diese Bachelorarbeit mit einer zusätzlichen räumlichen Begrenzung des Kristalls, den Quantum Wells.

Die gebundenen Zustände aus Elektron und Loch lassen sich dabei in erster Näherung als wasserstoffähnlich beschreiben. Als numerischer Lösungsansatz der wasserstoffähnlichen Beschreibung, mit Quantum Wells, dient dabei ein bereits implementiertes Programm.

Für eine detailliertere Beschreibung der Excitonzustände muss allerdings zusätzlich die Kristallstruktur berücksichtigt werden. Als bekannter Ansatz zur Berücksichtigung der Bandstruktur von Cu_2O sei der Suzuki-Hensel-Hamiltonian gewählt. Die freien Parameter werden dabei über einen Fit des Hamiltonians an eine Simulation der spin-DFT bestimmt. Da die naive Diagonalisierung des resultierenden Hamiltonians mit dem bereits bekannten Programm keine adäquate Rechenzeit liefern würde, müssen zunächst sowohl das Programm, als auch der Hamiltonian modifiziert werden. Die numerische Optimierung wird dabei zeitgleich in einer weiteren Bachelorarbeit am ITP1 angesetzt.

Diese Bachelorabreit beschäftigt sich hingegen mit einer analytischen Betrachtung des Hamiltonians. Ziel ist es, die Freiheitsgrade des Hamiltonians über die gegebenen Symmetrieen zu reduzieren, und damit die benötigte Rechenzeit zu minimieren.

Ausgangspunkt der Bachelorarbeit ist der von den zwölf Freiheitsgrade $\{x_\mathrm{e}, y_\mathrm{e}, z_\mathrm{e}, x_\mathrm{h}, y_\mathrm{h}, z_\mathrm{h}, I, S_\mathrm{h}\}$ abhängige Hamiltonian, in dreidimensionalen, kartesischen Koordinaten. Obwohl die Translationssymmetrie entlang der z-Achse durch die eingeführten Quantum Wells zerstört wird, bleibt sie weiterhin innerhalb der xy-Ebene erhalten. Durch die Einführung zweidimensionaler Realtiv- und Schwerpunktskoordinaten innerhalb der xy-Ebene, ergeben sich die zwölf Freiheitsgrade $\{x, y, X, Y, z_\mathrm{e}, z_\mathrm{h}, I, S_\mathrm{h}\}$. Die Wahl des Schwerpunktssystem, als Bezugssystem, setzt dabei $P_X = P_Y = 0$ und reduziert das System auf die zehn Freiheitsgrade $\{x, y, z_\mathrm{e}, z_\mathrm{h}, I, S_\mathrm{h}\}$.

Im Fall der wasserstoffähnlichen Beschreibung könnten die Freiheitsgrade durch Nutzen der Rotationssymmetrie innerhalb der xy-Ebene weiter reduziert werden. Diese kontinuierliche Symmetrie wird allerdings durch die Bandstruktur auf eine vierzählige, diskrete Symmetrie heruntergebrochen. Als Folge dessen bleibt bei der Transformation in Zylinderkoordinaten die ϕ Abhängigkeit des Hamiltonians erhalten. Die Transformation wird dennoch ausgeführt, da die verbleibende Punktsymmetrie den numerischen Aufwand weiter reduziert. Es ergeben sich schließlich die zehn Freiheitsgrade $\{\rho, \phi, z_\mathrm{e}, z_\mathrm{h}, I, S_\mathrm{h}\}$.

Kontrolliert wurde die Rechnung sowohl über einen Test der diskreten Rotationssymmetrie, als auch über Mathematica. Als Ausblick wurde eine geeignete Basis zur Diagionalisierung des Hamiltonians skizziert, wobei die Wahl der B-spline Funktionen durch eine vorherige Bachelorarbeit motiviert ist. In Zukunft soll damit die numerische Lösung der Exzitonzustände mit Berücksichtigung der Bandstruktur und der räumlichen Beschränkung durch Quantum Wells ermöglicht werden.

A Appendix

A.1 Hydrogen Atom

This section is based on References [**13-15**].

This section serves for a better understanding of quantum mechanically described bound states. The exact, analytical solution of the hydrogen atom motivates the physically interpretable quantum numbers, which are sufficient to describe the bound state. Furthermore, the solution of the differential equations via series expansions and the demand for normalisable states leads directly to the discrete nature of quantum mechanics. As a result, we obtain discrete eigenenergies and, especially for the ground state, the binding energy of the hydrogen atom and the corresponding Bohr radius, which enables a later comparison with the exciton states.

So before we introduce the excitons, let us take a look at the non-relativistic hydrogen atom. We consider the reference frame in which the proton rests and solve the Schrödinger equation for the possible electron states $\Psi(\boldsymbol{r}, t)$. The potential

$$V(\boldsymbol{r}) = \frac{-e^2}{4\pi\epsilon_0|\boldsymbol{r}|} \tag{A.1}$$

is thus independent of time. In order to find wave functions

$$\Psi(\boldsymbol{r}, t) = \sum_n c_n \psi_n(\boldsymbol{r}) \exp\{-iE_n t/\hbar\}, \tag{A.2}$$

which satisfy both the stationary Schrödinger equation (2.4) and the non-stationary Schrödinger equation

$$i\hbar\frac{\partial}{\partial t}\Psi = \Big(-\frac{\hbar^2\Delta}{2m} + V\Big)\Psi = \boldsymbol{H}\Psi \tag{A.3}$$

a product of a location-dependent wave function $\psi(\boldsymbol{r})$ and an exponential function is applied. The exponential function $\exp\{-iE_n t\hbar^{-1}\}$ describes the development of the wave function in time. Due to the spherical symmetry of the problem, it is advisable to continue the consideration in spherical coordinates. Consider the new representation of the Laplace operator

$$\Delta = \frac{1}{r^2}\frac{\partial}{\partial r}\left(r^2\frac{\partial}{\partial r}\right) + \frac{1}{r^2\sin\theta}\frac{\partial}{\partial\theta}\left(\sin\theta\frac{\partial}{\partial\theta}\right) + \frac{1}{r^2\sin^2\theta}\frac{\partial^2}{\partial\phi^2}. \tag{A.4}$$

In order to determine the location-dependent wave function, the stationary Schrödinger equation must be solved in spherical coordinates. A common approach is the separation of variables $\psi(r,\theta,\phi) = R(r)Y(\theta,\phi)$. When the Laplace operator Δ is inserted into equation (2.4), the expression

$$\begin{aligned} &\frac{-\hbar^2}{2m}\Big[\frac{Y}{r^2}\frac{\partial}{\partial r}\left(r^2\frac{\partial R}{\partial r}\right) + \frac{R}{r^2\sin\theta}\frac{\partial}{\partial\theta}\left(\sin\theta\frac{\partial Y}{\partial\theta}\right) \\ &+ \frac{R}{r^2\sin^2\theta}\left(\frac{\partial^2 Y}{\partial\phi^2}\right)\Big] + VRY = ERY \\ \Leftrightarrow\ A(r) \equiv &\Big[\frac{1}{R}\frac{\partial}{\partial r}\left(r^2\frac{\partial R}{\partial r}\right) + \frac{2mr^2}{\hbar^2}[E-V]\Big] \\ = &-\frac{1}{Y}\Big[\frac{1}{\sin\theta}\frac{\partial}{\partial\theta}\left(\sin\theta\frac{\partial Y}{\partial\theta}\right) + \frac{1}{\sin^2\theta}\frac{\partial^2 Y}{\partial\phi^2}\Big] \equiv -B(\theta,\phi) \end{aligned} \tag{A.5}$$

is obtained. Since both sides of the equation (A.5) have independent variables, $A(r)$ and $B(\theta,\phi)$ are constant. Choosing $A(r) = -B(\theta,\phi) \equiv l(l+1)$, results in two separeted differential equations. The differential equation

$$\frac{1}{R}\frac{\partial}{\partial r}\left(r^2\frac{\partial R}{\partial r}\right) + \frac{2mr^2}{\hbar^2}[V-E] = l(l+1) \tag{A.6}$$

describes the radial probability density $R(r)$ of the electron. Rewriting the partial derivatives

$$\frac{1}{R}\frac{\partial}{\partial r}\left(r^2\frac{\partial R}{\partial r}\right) = \frac{r}{R}\frac{\partial^2(rR)}{\partial r^2} \tag{A.7}$$

suggests to substitute further $U(r) = rR(r)$. The equation

$$\frac{d^2U}{dr^2} = \Big[\frac{l(l+1)}{r^2} - \frac{2mE}{\hbar^2} - \frac{me^2}{2\pi\epsilon_0\hbar^2 r}\Big]U \tag{A.8}$$

is in the form of a stationary Schrödinger equation with an additional term, which can be interpreted as a centrifugal potential. Since the differential equation only depends on one variable, the partial derivatives were replaced by total derivatives. Further replace $r = (4\pi\epsilon_0\hbar^2\rho)(me^2)^{-1}$, $E = (me^4)(32\pi^2\epsilon_0^2\hbar^2)\epsilon$ and write

$$\frac{d^2U}{d\rho^2} = \Big[-\epsilon - \frac{2}{\rho} + \frac{l(l+1)}{\rho^2}\Big]U. \tag{A.9}$$

A motivation for the form of $U(\rho)$ is provided by two special cases. For $\rho \to \infty$, equation (A.9) tends to

$$\frac{d^2U}{d\rho^2} \approx -\epsilon U \tag{A.10}$$

which is solved via the approach $U(\rho) = A\exp\{-\rho\sqrt{-\epsilon}\} + B\exp\{\rho\sqrt{-\epsilon}\}$. To obtain bound solutions, let $B = 0$. For $\rho \to 0$, equation (A.9) tends to

$$\frac{d^2U}{d\rho^2} \approx \frac{l(l+1)}{\rho^2}U \tag{A.11}$$

with the solution $U(\rho) = C\rho^{l+1}$. Note that by considering bound states we choose $E < 0$ and therefore $\sqrt{-\epsilon}$ is real. Introduce a function $\nu(\rho)$ such that

$$U(\rho) = \rho^{l+1}\exp\{-\rho\sqrt{-\epsilon}\}\nu(\rho). \tag{A.12}$$

The resulting differential equation

$$\rho\frac{d^2\nu}{d\rho^2} + 2(l+1-\sqrt{-\epsilon}\rho)\frac{d\nu}{d\rho} + 2(1-\sqrt{-\epsilon}(l+1))\nu = 0 \tag{A.13}$$

can be solved by the series approach

$$\nu = \sum_{j=0}^{\infty} a_j\rho^j. \tag{A.14}$$

With equation (A.14) and the partial derivatives

$$\begin{aligned} \frac{d\nu}{d\rho} &= \sum_{j=1}^{\infty} j a_j \rho^{j-1} = \sum_{j=0}^{\infty} (j+1) a_{j+1} \rho^j, \\ \frac{d^2\nu}{d\rho^2} &= \sum_{j=1}^{\infty} j(j+1) a_{j+1} \rho^{j-1}, \end{aligned} \tag{A.15}$$

inserted into equation (A.13) the coefficients

$$a_{j+1} = \Big[-\frac{2(-\sqrt{-\epsilon}(j+l+1)+1)}{(j+1)(j+2l+2)} a_j \Big] \tag{A.16}$$

are determined recursively. Consider the asymptotic behaviour of $\nu(\rho)$ with the coefficients $a_{j+1} = 2\sqrt{-\epsilon}/(j+1)a_j$ for $j \to \infty$. Assuming that the equation

$$\lim_{j\to\infty} \frac{a_{j+1}}{a_j} = \frac{2\sqrt{-\epsilon}}{j+1}, \tag{A.17}$$

is valid for any j, the coefficients result in

$$a_j = \frac{(2\sqrt{-\epsilon})^j}{j!} a_0. \tag{A.18}$$

If one identifies this expression as an exponential serie,

$$a_0 \sum_{j=1}^{\infty} \frac{(2\sqrt{-\epsilon})^j}{j!} \rho^j = a_0 \exp\big\{2\sqrt{-\epsilon}\rho\big\} \tag{A.19}$$

follows directly. Therefore $\nu(\rho)$, $U(r)$, and finally $R(r)$ would diverge. To avoid the divergence of

$$R_{nl}(r) = \frac{1}{r} \rho^{l+1} \exp\big\{-\sqrt{-\epsilon}\rho\big\} \nu(\rho) \tag{A.20}$$

for large j, there must be a $j_{\max}$, so that $j > j_{\max}$ implies $a_j = 0$. The condition $a_{\max} + 1 = 0$ yields the relation $-\sqrt{-\epsilon}(j_{max} + l + 1) + 1 = 0$. Define $n := j_{\max} + l + 1$ to obtain discrete energy values

$$E_n = -\frac{me^2}{32\pi\hbar^2\epsilon_0}\frac{1}{n^2} = \frac{-13.6\text{eV}}{n^2}. \tag{A.21}$$

The obtained Bohr's formula is one of the greatest achievements in quantum mechanics. Using a semiclassical approach to the conservation of energy

$$E_{n=1}(r_0) = -\frac{me^4}{32\pi^2\epsilon_0^2\hbar^2} = \frac{\hbar^2}{2mr_0^2} - \frac{e^2}{4\pi\epsilon_0 r_0} = T(r_0) + V(r_0), \tag{A.22}$$

with the kinetic energy T, and the potential V, the Bohr radius

$$r_0 = \frac{4\pi\epsilon_0\hbar^2}{me^2} \approx 5.29 \times 10^{-11}\text{m} \tag{A.23}$$

can also be determined. Taking into account the termination condition to further identify

$$\nu(\rho) = L_{n-l-1}^{2l+1}(2\rho) \tag{A.24}$$

then the radial probability distribution

$$R_{nl}(r) = c_{nl}\frac{\rho^l}{r}\exp\{-\sqrt{-\epsilon}\rho\}L_{n-l-1}^{2l+1}(2\rho) \tag{A.25}$$

with the normalisation constant c_{nl} is obtained.

$$L_{n-l-1}^{2l+1}(x) = \sum_{j=0}^{n-l-1}(-1)^j\binom{n+l}{n-l-1-j}\frac{x^j}{j!} \tag{A.26}$$

are the Laguerre polynomials, which represent the remaining exponential terms.

Since solving the angular-dependent differential equations does not yield energy values, the following solution path is less detailed, but still motivates the occuring quantum numbers. A separation of the variables $Y(\theta, \phi) = \Theta(\theta)\Phi(\phi)$ is also used for the differential equation

$$\frac{1}{Y}\Big[\frac{1}{\sin\theta}\frac{\partial}{\partial\theta}\Big(\sin\theta\frac{\partial Y}{\partial\theta}\Big)+\frac{1}{\sin^2\theta}\frac{\partial^2 Y}{\partial\phi^2}\Big]=-l(l+1). \tag{A.27}$$

The separation $Y=\Phi\Theta$ leads again to two constant terms

$$\begin{aligned}-\frac{\Phi}{\sin\theta}\frac{\partial}{\partial\theta}\Big(\sin\theta\frac{\partial\Theta}{\partial\theta}\Big)-\frac{\Phi}{\sin^2\theta}\frac{\partial^2\Phi}{\partial\phi^2}&=l(l+1)\Theta\Phi\\ \Leftrightarrow -\frac{\sin\theta}{\Theta}\frac{\partial}{\partial\theta}\Big(\sin\theta\frac{\partial\Theta}{\partial\theta}\Big)-l(l+1)\sin^2\theta&=\frac{1}{\Phi}\frac{\partial^2\Phi}{\partial\phi^2}\equiv -m^2\end{aligned} \tag{A.28}$$

that can be considered separately. This time $-m^2$ is chosen as the constant. The differential equation

$$\frac{\partial^2\Phi}{\partial\phi^2}=-m^2\Phi \tag{A.29}$$

for the ϕ dependent part is solved using the approach $\Phi=A\exp\{im\phi\}+B\exp\{-im\phi\}$. Since ϕ is cyclic ($\Phi(\phi)=\Phi(\phi+2\pi)$) and therefore holds the condition $\exp\{\pm 2i\pi m\}=1$, $m\in\{0,\pm1,\pm2,...,\pm(l-1),\pm l\}$ takes integer values. Due to the selection option for m, we are free to set $B=0$. After a normalisation,

$$\Phi=\frac{1}{\sqrt{2\pi}}\exp\{im\phi\} \tag{A.30}$$

results. The θ dependent differential equation

$$\begin{aligned}-\frac{\Theta}{\sin\theta}\frac{\partial}{\partial\theta}\Big(\sin\theta\frac{\partial\Theta}{\partial\theta}\Big)-l(l+1)\sin^2\theta&=-m^2\\ \Leftrightarrow \frac{1}{\sin\theta}\frac{\partial}{\partial\theta}\Big(\sin\theta\frac{\partial\Theta}{\partial\theta}\Big)+\Big(l(l+1)-\frac{m^2}{\sin^2\theta}\Big)\Theta&=0\end{aligned} \tag{A.31}$$

with the entries $\sin\theta$ and $\sin^2\theta$ can be solved by a series expansion of $\sin\theta$ and $\cos\theta$. Therefore substitute $\xi=\cos\theta$ to get

$$\frac{\partial}{\partial\xi}\Big[(1-\xi^2)\frac{\partial\Theta}{\partial\xi}\Big]+\Big[l(l+1)-\frac{m^2}{(1-\xi^2)}\Big]\Theta=0. \tag{A.32}$$

Since the differential equation is still difficult to solve, a further substitution

$$\Theta = (1 - \xi^2)^{\frac{|m|}{2}} G(\xi). \tag{A.33}$$

is used. It should be noted that this non-trivial and also non-obvious substitution is a common substitution for advanced differential equation solving. Now the series expansion

$$G(\xi) = \sum_{n=0}^{\infty} b_n \xi^n. \tag{A.34}$$

is used. The determination of the coefficients b_n can be followed in reference **[13]**, in section 6.5.2. As before, a termination condition of the coefficients is required to avoid divergence of the series. The solution

$$\Theta_{lm}(\theta) = \sqrt{\frac{(2l+1)(l-m)!}{2(l+m)!}} P_{lm}(\cos\theta), \tag{A.35}$$

contains the Legendre polynomials

$$P_{lm}(\xi) = \frac{1}{2^l l!}(1 - \xi^2)^{\frac{m}{2}} \frac{\partial^{l+m}(\xi^2 - 1)^l}{\partial \xi^{l+m}}. \tag{A.36}$$

and leads to the spherical harmonics functions $Y_{ml}(\theta, \phi)$. In total, the wave function

$$\psi_{nlm}(r, \theta, \phi) = R_{nl}(r) Y_{lm}(\theta, \phi), \tag{A.37}$$

determined by three quantum numbers n, l, m represents the electron state in the hydrogen atom.

A.2 Partial Derivatives

Used partial derivatives to transform between Cartesian coordinates (x, y) and plane polar coordinates (ρ, ϕ).

$$\frac{\partial}{\partial \rho} = \frac{\partial x}{\partial \rho}\frac{\partial}{\partial x} + \frac{\partial y}{\partial \rho}\frac{\partial}{\partial y} = \cos\phi\frac{\partial}{\partial x} + \sin\phi\frac{\partial}{\partial y}, \tag{A.38}$$

$$\begin{aligned}
\frac{\partial^2}{\partial \rho^2} =& \Big(\cos\phi\frac{\partial}{\partial x} + \sin\phi\frac{\partial}{\partial y}\Big)\Big(\cos\phi\frac{\partial}{\partial x} + \sin\phi\frac{\partial}{\partial y}\Big) \\
=& \cos\phi\Big[\frac{\partial}{\partial x}\Big(\cos\phi\frac{\partial}{\partial x}\Big) + \frac{\partial}{\partial x}\Big(\sin\phi\frac{\partial}{\partial y}\Big)\Big] \\
&+ \sin\phi\Big[\frac{\partial}{\partial y}\Big(\cos\phi\frac{\partial}{\partial x}\Big) + \frac{\partial}{\partial y}\Big(\sin\phi\frac{\partial}{\partial y}\Big)\Big] \\
=& \cos\phi\Big[\frac{\sin^2\phi}{\rho}\frac{\partial}{\partial x} + \cos\phi\frac{\partial^2}{\partial x^2} - \frac{\cos\phi\sin\phi}{\rho}\frac{\partial}{\partial y} + \sin\phi\frac{\partial}{\partial x}\frac{\partial}{\partial y}\Big] \\
&+ \sin\phi\Big[-\frac{\sin\phi\cos\phi}{\rho}\frac{\partial}{\partial x} + \cos\phi\frac{\partial}{\partial x}\frac{\partial}{\partial y} + \frac{\cos^2\phi}{\rho^2}\frac{\partial}{\partial y} + \sin\phi\frac{\partial^2}{\partial y^2}\Big] \\
=& \cos^2\phi\frac{\partial^2}{\partial x^2} + \sin^2\phi\frac{\partial^2}{\partial y^2} + 2\sin\phi\cos\phi\frac{\partial}{\partial x}\frac{\partial}{\partial y},
\end{aligned} \tag{A.39}$$

$$\frac{\partial}{\partial \phi} = \frac{\partial x}{\partial \phi}\frac{\partial}{\partial x} + \frac{\partial y}{\partial \phi}\frac{\partial}{\partial y} = -\rho\sin\phi\frac{\partial}{\partial x} + \rho\cos\phi\frac{\partial}{\partial y}, \tag{A.40}$$

$$
\begin{aligned}
\frac{\partial^2}{\partial\phi^2} =& \Big(-\rho\sin\phi\frac{\partial}{\partial x}+\rho\cos\phi\frac{\partial}{\partial y}\Big)\Big(-\rho\sin\phi\frac{\partial}{\partial x}+\rho\cos\phi\frac{\partial}{\partial y}\Big)\\
=& -\rho\sin\phi\Big[\frac{\partial}{\partial x}\Big(-\rho\sin\phi\frac{\partial}{\partial x}\Big)+\frac{\partial}{\partial x}\Big(\rho\cos\phi\frac{\partial}{\partial y}\Big)\Big]\\
&+\rho\cos\phi\Big[\frac{\partial}{\partial y}\Big(-\rho\sin\phi\frac{\partial}{\partial x}\Big)+\frac{\partial}{\partial y}\Big(\rho\cos\phi\frac{\partial}{\partial y}\Big)\Big]\\
=& -\rho\sin\phi\Big[\Big(\sin\phi\cos\phi-\frac{\sin\phi\cos\phi}{\rho}\Big)\frac{\partial}{\partial x}-\rho\sin\phi\frac{\partial^2}{\partial x^2}\\
&+\Big(\frac{\cos^2\phi}{\rho}+\sin^2\phi\Big)\frac{\partial}{\partial y}+\rho\cos\phi\frac{\partial}{\partial x}\frac{\partial}{\partial y}\Big]\\
&+\rho\cos\phi\Big[\Big(-\cos^2\phi-\frac{\sin^2\phi}{\rho}\Big)\frac{\partial}{\partial x}-\rho\sin\phi\frac{\partial}{\partial x}\frac{\partial}{\partial y}\\
&+\Big(\frac{\sin\phi\cos\phi}{\rho}-\sin\phi\cos\phi\Big)\frac{\partial}{\partial y}+\rho\cos\phi\frac{\partial^2}{\partial y^2}\Big]\\
=&\rho^2\sin^2\phi\frac{\partial^2}{\partial x^2}+\rho^2\cos^2\phi\frac{\partial^2}{\partial y^2}-\rho\cos\phi\frac{\partial}{\partial x}\\
&-\rho\sin\phi\frac{\partial}{\partial y}-2\rho^2\sin\phi\cos\phi\frac{\partial}{\partial x}\frac{\partial}{\partial y},
\end{aligned}
\tag{A.41}
$$

$$
\frac{\partial^2}{\partial x^2}+\frac{\partial^2}{\partial y^2}=\frac{\partial^2}{\partial\rho^2}+\frac{1}{\rho^2}\frac{\partial^2}{\partial\phi^2}+\frac{1}{\rho}\frac{\partial}{\partial\rho},
\tag{A.42}
$$

$$
\frac{\partial}{\partial x}=\frac{\partial\rho}{\partial x}\frac{\partial}{\partial\rho}+\frac{\partial\phi}{\partial x}\frac{\partial}{\partial\phi}=\cos\phi\frac{\partial}{\partial\rho}-\frac{\sin\phi}{\rho}\frac{\partial}{\partial\phi},
\tag{A.43}
$$

$$
\begin{aligned}
\frac{\partial^2}{\partial x^2} =&(\cos\phi\frac{\partial}{\partial\rho} - \frac{\sin\phi}{\rho}\frac{\partial}{\partial\phi})(\cos\phi\frac{\partial}{\partial\rho} - \frac{\sin\phi}{\rho}\frac{\partial}{\partial\phi}) \\
&= \cos\phi\Big[\cos\phi\frac{\partial^2}{\partial\rho^2} - \frac{\partial}{\partial\rho}\Big(\frac{\sin\phi}{\rho}\Big)\frac{\partial}{\partial\phi} - \frac{\sin\phi}{\rho}\frac{\partial}{\partial\phi}\frac{\partial}{\partial\rho}\Big] \\
&\quad - \frac{\sin\phi}{\rho}\Big[\Big(\frac{\partial}{\partial\phi}\cos\phi\Big)\frac{\partial}{\partial\rho} + \cos\phi\frac{\partial}{\partial\rho}\frac{\partial}{\partial\phi} \\
&\quad - \frac{\partial}{\partial\phi}\Big(\frac{\sin\phi}{\rho}\Big)\frac{\partial}{\partial\phi} - \frac{\sin\phi}{\rho}\frac{\partial^2}{\partial\phi^2}\Big] \\
&= \cos^2\phi\frac{\partial^2}{\partial\rho^2} + \frac{2\cos\phi\sin\phi}{\rho^2}\frac{\partial}{\partial\phi} - \frac{2\cos\phi\sin\phi}{\rho}\frac{\partial}{\partial\phi}\frac{\partial}{\partial\rho} \\
&\quad + \frac{\sin^2\phi}{\rho}\frac{\partial}{\partial\rho} + \frac{\sin^2\phi}{\rho^2}\frac{\partial^2}{\partial\phi^2},
\end{aligned}
\tag{A.44}
$$

$$
\frac{\partial}{\partial y} = \frac{\partial\rho}{\partial y}\frac{\partial}{\partial\rho} + \frac{\partial\phi}{\partial y}\frac{\partial}{\partial\phi} = \sin\phi\frac{\partial}{\partial\rho} + \frac{\cos\phi}{\rho}\frac{\partial}{\partial\phi}, \tag{A.45}
$$

$$
\begin{aligned}
\frac{\partial^2}{\partial y^2} =&(\sin\phi\frac{\partial}{\partial\rho} + \frac{\cos\phi}{\rho}\frac{\partial}{\partial\phi})(\sin\phi\frac{\partial}{\partial\rho} + \frac{\cos\phi}{\rho}\frac{\partial}{\partial\phi}) \\
&= \sin\phi\Big[\sin\phi\frac{\partial^2}{\partial\rho^2} + \Big(\frac{\partial}{\partial\rho}\frac{\cos\phi}{\rho}\Big)\frac{\partial}{\partial\phi} + \frac{\cos\phi}{\rho}\frac{\partial}{\partial\phi}\frac{\partial}{\partial\rho}\Big] \\
&\quad + \frac{\cos\phi}{\rho}\Big[\frac{\partial}{\partial\phi}\frac{\partial}{\partial\rho} + \sin\phi\frac{\partial}{\partial\phi}\frac{\partial}{\partial\rho} + \Big(\frac{\partial}{\partial\phi}\frac{\cos\phi}{\rho}\Big)\frac{\partial}{\partial\phi} + \frac{\cos\phi}{\rho}\frac{\partial^2}{\partial\phi^2}\Big] \\
&= \sin^2\phi\frac{\partial^2}{\partial\rho^2} - \frac{2\sin\phi\cos\phi}{\rho^2}\frac{\partial}{\partial\phi} + \frac{2\sin\phi\cos\phi}{\rho}\frac{\partial}{\partial\phi}\frac{\partial}{\partial\rho} \\
&\quad + \frac{\cos^2\phi}{\rho}\frac{\partial}{\partial\rho} + \frac{\cos^2\phi}{\rho^2}\frac{\partial^2}{\partial\phi^2},
\end{aligned}
\tag{A.46}
$$

$$\begin{aligned}
\frac{\partial}{\partial y}\frac{\partial}{\partial x} =& \frac{\partial}{\partial x}\frac{\partial}{\partial y} = (\sin\phi\frac{\partial}{\partial\rho} + \frac{\cos\phi}{\rho}\frac{\partial}{\partial\phi})(\cos\phi\frac{\partial}{\partial\rho} - \frac{\sin\phi}{\rho}\frac{\partial}{\partial\phi}) \\
&= \sin\phi\Big[\cos\phi\frac{\partial^2}{\partial\rho^2} - \Big(\frac{\partial}{\partial\rho}\frac{\sin\phi}{\rho}\Big)\frac{\partial}{\partial\phi} - \frac{\sin\phi}{\rho}\frac{\partial}{\partial\rho}\frac{\partial}{\partial\phi}\Big] \\
&\quad + \frac{\cos\phi}{\rho}\Big[\Big(\frac{\partial}{\partial\phi}\cos\phi\Big)\frac{\partial}{\partial\rho} + \cos\phi\frac{\partial}{\partial\rho}\frac{\partial}{\partial\phi} - \Big(\frac{\sin\phi}{\rho}\Big)\frac{\partial}{\partial\phi} - \frac{\sin\phi}{\rho}\frac{\partial^2}{\partial\phi^2}\Big] \qquad \text{(A.47)} \\
&= \sin\phi\cos\phi\frac{\partial^2}{\partial\rho^2} + \frac{\sin^2\phi - \cos^2\phi}{\rho^2}\frac{\partial}{\partial\phi} + \frac{\cos^2\phi - \sin^2\phi}{\rho}\frac{\partial}{\partial\rho}\frac{\partial}{\partial\phi} \\
&\quad - \frac{\sin\phi\cos\phi}{\rho}\frac{\partial}{\partial\rho} - \frac{\sin\phi\cos\phi}{\rho^2}\frac{\partial^2}{\partial\phi^2}.
\end{aligned}$$

A.3 Mathematica Code

Mathematica code for comparsion with the analytical calculation.

```
pxpx[\[Rho]_, \[Phi]_] := (px[\[Rho], \[Phi]] [
    px[\[Rho], \[Phi]] [#]]) &
pypy[\[Rho]_, \[Phi]_] := (py[\[Rho], \[Phi]] [
    py[\[Rho], \[Phi]] [#]]) &
pxpy[\[Rho]_, \[Phi]_] := (px[\[Rho], \[Phi]] [
    py[\[Rho], \[Phi]] [#]]) &

n1[\[Rho]_, \[Phi]_] := (a1*(pxpx[\[Rho], \[Phi]][#] +
      pypy[\[Rho], \[Phi]][#]) -
   a2 (i1i1*pxpx[\[Rho], \[Phi]][#] + i2i2*pypy[\[Rho], \[Phi]][#]) -
   a3 (pxpy[\[Rho], \[Phi]][#]))
n2[\[Rho]_, \[Phi]_] := (b1*py[\[Rho], \[Phi]][#] +
    b2*px[\[Rho], \[Phi]][#]) &
m1[\[Rho]_, \[Phi]_] := (c1*(pxpx[\[Rho], \[Phi]][#] +
       pypy[\[Rho], \[Phi]][#]) -
    c2*(i1s1*pxpx[\[Rho], \[Phi]][#] + i2s2*pypy[\[Rho], \[Phi]][#]) -
```

```
     c3*(pxpy[\[Rho], \[Phi]][#])) &
m2[\[Rho]_, \[Phi]_] := (d1*py[\[Rho], \[Phi]][#] +
    d2*px[\[Rho], \[Phi]][#]) &

a1 := (\[Gamma]1'/2/m0 + 2*\[Gamma]2/m0)
a2 := 3*\[Gamma]2/m0
a3 := 6*\[Gamma]3/m0*i1i2
b1 := 6*\[Gamma]3/m0*phz*i2i3
b2 := 6*\[Gamma]3/m0*phz*i3i1
c1 := (\[Eta]1 + 2*\[Eta]2)/m0*i*s
c2 := 6*\[Eta]2/m0
c3 := 6*\[Eta]3/m0*(i1s2 + i2s1)
d1 := 6*\[Eta]3/m0*phz*(i2s3 + i3s2)
d2 := 6*\[Eta]3/m0*phz*(i3s1 + i1s3)

Simplify[n1[\[Rho], \[Phi]][\[Psi][\[Rho], \[Phi]]] +
  n2[\[Rho], \[Phi]][\[Psi][\[Rho], \[Phi]]] +
  m1[\[Rho], \[Phi]][\[Psi][\[Rho], \[Phi]]] +
  m2[\[Rho], \[Phi]][\[Psi][\[Rho], \[Phi]]]]
FullSimplify[
 n1[\[Rho], \[Phi]][\[Psi][\[Rho], \[Phi]]] +
  n2[\[Rho], \[Phi]][\[Psi][\[Rho], \[Phi]]] +
  m1[\[Rho], \[Phi]][\[Psi][\[Rho], \[Phi]]] +
  m2[\[Rho], \[Phi]][\[Psi][\[Rho], \[Phi]]]]
```

A.4 Symmetry Test

Result of the discrete symmetry test, by inserting $(\phi, \rho) \to (\phi' - \pi/2, \rho')$, and $(I_1, I_2, S_{\mathrm{h}1}, S_{\mathrm{h}2}) \to (I_2, -I_1, S_{\mathrm{h}2}, -S_{\mathrm{h}1})$ into the Hamiltonian (4.50)

$$
\begin{aligned}
H =& E_{\mathrm{g}} + H_{\mathrm{SO}} - \frac{1}{4\pi\epsilon_0}\frac{1}{\sqrt{\rho^2 + (z_{\mathrm{e}} - z_{\mathrm{h}})^2}} + V_{\mathrm{e}}(z_{\mathrm{e}}) + V_{\mathrm{h}}(z_{\mathrm{h}}) \\
& \frac{1}{2\hbar^2 m_0}\Big[\hbar^2(\gamma_1 + 4\gamma_2) - 6\gamma_2 I_3^2 + 2\boldsymbol{I}\boldsymbol{S}_{\mathrm{h}}(\eta_1 + 2\eta_2) - 12 I_3 S_{\mathrm{h}3}\Big] p_{\mathrm{hz}}^2 + \frac{1}{2m_{\mathrm{e}}} p_{\mathrm{ez}}^2 \\
& + \frac{i}{2\hbar m_0}\Big[-\hbar^2(\gamma_1' + 4\gamma_2) - 2\boldsymbol{I}\boldsymbol{S}_{\mathrm{h}}(\eta_1 + 2\eta_2) + 6\gamma_2(I_2^2\cos^2\phi + I_1^2\sin^2\phi) \\
& + 12\eta_2(I_2 S_{\mathrm{h}2}\cos^2\phi + I_1 S_{\mathrm{h}1}\sin^2\phi) + 6\sin 2\phi(-\gamma_3\{I_2, I_1\} \\
& - \eta_3(I_2 S_{\mathrm{h}1} + I_1 S_{\mathrm{h}2}))\Big]\frac{1}{\rho} p_\rho \\
& + \frac{6}{\hbar^2 m_0}\Big[-\sin\phi(-\gamma_3\{I_3, I_2\} - \eta_3(I_3 S_{\mathrm{h}2} + I_2 S_{\mathrm{h}3}) \\
& + \cos\phi(\gamma_3\{I_1, I_3\} + \eta_3(I_1 S_{\mathrm{h}3} + I_3 S_{\mathrm{h}1}))\Big] p_{\mathrm{hz}} p_\rho \\
& + \frac{3i}{\hbar m_0}\Big[-\sin 2\phi(\gamma_2(I_2^2 - I_1^2) + 2\eta_2(I_2 S_{\mathrm{h}2} - I_1 S_{\mathrm{h}1})) \\
& + 2\cos 2\phi(-\gamma_3\{I_2, I_1\} - \eta_3(I_2 S_{\mathrm{h}1} + I_1 S_{\mathrm{h}2}))\Big]\frac{1}{\rho^2} p_\phi \\
& + \frac{6}{\hbar^2 m_0}\Big[-\sin\phi(\gamma_3\{I_1, I_3\} + \eta_3(I_1 S_{\mathrm{h}3} + I_3 S_{\mathrm{h}1})) \\
& - \cos\phi(-\gamma_3\{I_3, I_2\} - \eta_3(I_3 S_{\mathrm{h}2} + I_2 S_{\mathrm{h}3}))\Big]\frac{p_{\mathrm{hz}}}{\rho} p_\phi
\end{aligned}
\tag{A.48}
$$

$$+\frac{1}{2\hbar^2 m_0}\Big[\hbar^2(\gamma_1'+4\gamma_2)+2\boldsymbol{I}\boldsymbol{S}_{\mathrm{h}}(\eta_1+2\eta_2)-6\gamma_2(I_2^2\sin^2\phi+I_1^2\cos^2\phi)$$

$$-12\eta_2(I_2 S_{\mathrm{h}2}\sin^2\phi+I_1 S_{\mathrm{h}1}\cos^2\phi)+6\sin 2\phi(-\gamma_3\{I_2,I_1\}$$

$$-\eta_3(I_2 S_{\mathrm{h}1}+I_1 S_{\mathrm{h}2}))\Big]p_\rho^2$$

$$+\frac{1}{2\hbar^2 m_0}\Big[\hbar^2(\gamma_1'+4\gamma_2)+2\boldsymbol{I}\boldsymbol{S}_{\mathrm{h}}(\eta_1+2\eta_2)-6\gamma_2(I_2^2\cos^2\phi+I_1^2\sin^2\phi)$$

$$-12\eta_2(I_2 S_{\mathrm{h}2}\cos^2\phi+I_1 S_{\mathrm{h}1}\sin^2\phi)-6\sin 2\phi(-\gamma_3\{I_2,I_1\}$$

$$-\eta_3(I_2 S_{\mathrm{h}1}+I_1 S_{\mathrm{h}2}))\Big]\frac{1}{\rho^2}p_\phi^2$$

$$+\frac{3}{\hbar^2 m_0}\Big[-\sin 2\phi(-\gamma_2(I_2^2-I_1^2)+2\eta_2(I_2 S_{\mathrm{h}2}-I_1 S_{\mathrm{h}1}))$$

$$+2\cos 2\phi(-\gamma_3\{I_2,I_1\}-\eta_3(I_2 S_{\mathrm{h}1}+I_1 S_{\mathrm{h}2}))\Big]\frac{1}{\rho}p_\rho p_\phi$$

It can thus be seen that a rotation by $\pi/2$ of the Hamiltonian, comparative to its original form (**??**) again yields identical terms. This shows the expected preservation of $C_4(z)$ symmetry and thus served as the first falsification test for the Hamiltonian.

Bibliography

[1] Frenkel, J.A. (1931). On the transformation of light into heat in solids. In *I. Phys. Rev. 37, 17.*

https://journals.aps.org/pr/pdf/10.1103/PhysRev.37.17

[2] Peierls, R. (1932). Zur Theorie der Absorptionsspektren fester Körper. In *Annalen der Physik 405, 905.* (DOI: 10.1002/andp.19324050803)

[3] Wannier, G.H. (1937). The structure of electronic excitation levels in insulating crystals. In *Phys. Rev. 52, 191.*

https://journals.aps.org/pr/pdf/10.1103/PhysRev.52.191

[4] Gross, E.F. and Karryjew I.A. (1952). The optical spectrum of the exciton. In *Dokl. Akad. Nauk. SSSR 84, 471.*

https://link.springer.com/content/pdf/10.1007/BF02746069.pdf?pdf=button

[5] Kazimierczuk, T. and Fröhlich, D. and Scheel, S. and Stolz, H. and Bayer, M. (2014). Giant Rydberg excitons in the copper oxide Cu2O. In *Nature 514, 343.*

https://www.nature.com/articles/nature13832

[6] Schweiner, F. (2017). Theory of excitons in cuprous oxide (PhD thesis). University of Stuttgart. (DOI: 10.18419/OPUS-9483)

[7] Belov, P.A. (2022). Linewidths and energy shifts of electron-impurity resonant states in quantum wells with infinite barriers. In *Phys. Rev. 105, 155417.* (DOI: 10.1103/PhysRevB.105.155417)

[8] Kühner, L. (2022). Computation of the transition from quantum wells to bulk exciton states of cuprous oxide using B-spline basis functions (Bachelor thesis). University of Stuttgart. (DOI: 10.18419/opus-12564)

[9] Hunklinger, S. and Enss, C. (2022). *Solid State Physics*. De Gruyter, Boston. (DOI: 10.1515/9783110666502)

[10] Rössler, U. (2009). *Solid State Theory: An Introduction*, Second Edition. Springer Berlin, Heidelberg. (DOI: 10.1007/978-3-540-92762-4)

[11] Zielinski, P. (2018) Berechnung hochangeregter Exzitonen in elektrischen und magnetischen Feldern mit der Methode der komplexen Koordinatenrotation (Master thesis). University of Stuttgart. (DOI: 10.18419/opus-10130)

[12] Jörger, M. (2004). Terahertzspektroskopie an Cu_2O: Intraexzitonische und phononische Übergänge (PhD thesis). Karlsruhe Institute of Technology.

[13] Reed, B.C. (2022). *Quantum Mechanics: An Enhanced Primer*, Second Edition. Springer Charm. (DOI: 10.1007/978-3-031-14020-4)

[14] Griffiths, D.J. and Schroeter, D.F (2018). *Introduction to Quantum Mechanics*, Third Edition. Cambridge University Press, Cambridge. (DOI: 10.1017/9781316995433)

[15] Wick, M. (2019). *Quantenmechanik mit Concept-Maps: Mit Struktur und Übersicht besser verstehen lernen*, First Edition. Springer Spektrum Berlin, Heidelberg. (DOI: 10.1007/978-3-662-59424-7)

[16] Hodby, J.W. and Jenkins, T.E. and Schwab, C. and Tamura, H. and Trivich, D. (1976). Cyclotron resonance of electrons and of holes in cuprous oxide, Cu_2O. In *Journal of Physics C: Solid State Physics 9.8*. (DOI: 10.1088/0022-3719/9/8/014)

[17] Madelung, O. and Rössler, U. and Schulz, M. (1998). Cuprous oxide Cu_2O dielectric constant: *Datasheet from Landolt-Börnstein - Group III Condensed Matter · Volume 41C: "Non-Tetrahedrally Bonded Elements and Binary Compounds I"*. Springer-Verlag, Berlin. (DOI: $10.1007/10681727_58$)

[18] Schöne, F. and Krüger, S.O. and Grünwald, P. and Stolz, H. and Scheel, S. and Aßmann, M. and Heckötter, J. and Thewes, J. and Fröhlich, D. and Bayer, M. (2016). Deviations of the exciton level spectrum in Cu_2O from the hydrogen series. In *Phys. Rev. B 93, 075203*. (DOI: 10.1103/PhysRevB.93.075203)

[19] Schweiner, F. and Main, J. and Feldmaier, M. and Wunner, G. (2016). Impact of the valence band structure of Cu_2O on excitonic spectra. In *Phys. Rev. B 93, 195203*. (DOI: 10.1103/PhysRevB.93.195203)

Danksagung

Hiermit möchte ich mich herzlich für die großzügige Unterstützung meiner Studienarbeit bedanken. Ein besonderer Dank gilt Dr. Patric Rommel und Prof. Jörg Main für ihre fachliche Expertise, tatkräftige Hilfe, und damit auch für die Ermöglichung meiner Arbeit. Ebenso möchte ich mich bei den weiteren Mitgliedern des 1. Instituts für Theoretische Physik für die angenehme Arbeitsatmosphäre und Hilfe jeglicher Art bedanken. Ich bin auch dankbar für meine Korrekturleser, ohne deren Hilfe meine Arbeit weit weniger präzise und verständlich formuliert wäre. Schließlich möchte ich mich noch bei meiner Familie bedanken, welche mir den erfolgreichen Abschluss meines Studiums erst ermöglicht hat.

Ich bedanke mich herzlichst bei allen Unterstützern für ihre Zeit und Mühe.

Erklärung

Ich versichere,

- dass ich diese Bachelorarbeit selbstständig verfasst habe,
- dass ich keine anderen als die angegebenen Quellen benutzt und alle wörtlich oder sinngemäß aus anderen Werken übernommenen Aussagen als solche gekennzeichnet habe,
- dass die eingereichte Arbeit weder vollständig noch in wesentlichen Teilen Gegenstand eines anderen Prüfungsverfahrens gewesen ist,
- und dass das elektronische Exemplar mit den anderen Exemplaren übereinstimmt.

Stuttgart, den 16.03.2023 *Frieder Pfeiffer*